

Neutron star mass in dark matter clumps

Maksym Deliyergiyev,^{1,2*} Antonino Del Popolo,^{3,4,5†} Morgan Le Delliou,^{6,7,8,9‡}

¹Department of Nuclear Particle Physics, University of Geneva, CH-1211, Switzerland

²High Performance Computing Center Stuttgart (HLRS), Universität Stuttgart, 70550 Stuttgart, Germany

³Dipartimento di Fisica e Astronomia, University Of Catania, Viale Andrea Doria 6, 95125, Catania, Italy

⁴Institute of Astronomy and National Astronomical Observatory, Bulgarian Academy of Sciences, 72, Tsarigradsko Shosse Blvd., 1784 Sofia, Bulgaria

⁵Institute of Astronomy, Russian Academy of Sciences, Pyatnitskaya street, 48, 119017 Moscow, Russia

⁶Institute of Theoretical Physics & Research Center of Gravitation, Lanzhou University, Lanzhou 730000, China

⁷Key Laboratory of Quantum Theory and Applications of MoE, Lanzhou University, Lanzhou 730000, China

⁸Lanzhou Center for Theoretical Physics & Key Laboratory of Theoretical Physics of Gansu Province, Lanzhou University, Lanzhou 730000, China

⁹Instituto de Astrofísica e Ciências do Espaço, Universidade de Lisboa, Faculdade de Ciências, Ed. C8, Campo Grande, 1769-016 Lisboa, Portugal

Accepted 2023 October 23. Received 2023 September 28; in original form 2023 May 31

ABSTRACT

This paper investigates a hypothesis proposed in previous research relating neutron star (NS) mass and its dark matter (DM) accumulation. As DM accumulates, NS mass decreases, predicting lower NS masses toward the Galactic center. Due to limited NSs data near the galactic center, we examine NSs located within DM clumps. Using the CLUMPY code simulations, we determine the DM clumps distribution, with masses from 10 to $10^8 M_{\odot}$ and scales from 10^{-3} to 10 kpc. These clumps' DM exhibit a peak at the center, tapering toward the outskirts, resembling our Galaxy's DM distribution. We analyse these DM clumps' NS mass variations, considering diverse DM particle masses and galaxy types. We find relatively stable NS mass within 0.01 to 5 kpc from the clump center. This stability supports the initial hypothesis, particularly for NSs located beyond 0.01 kpc from the clump center, where NS mass reaches a plateau around 0.1 kpc. Nevertheless, NS mass near the clump's periphery reveals spatial dependence: NS position within DM clumps influences its mass in Milky Way-type galaxies. Moreover, this dependence varies with the DM model considered. In summary, our study investigates the proposed link between NS mass and DM accumulation by examining NSs within DM clumps. While NS mass remains stable at certain distances from the clump center, spatial dependencies arise near the clump's outer regions, contingent on the specific DM model.

Key words: neutron stars – dark matter – sky map – dark matter halo – clumps – microhaloes – minihaloes

1 INTRODUCTION

Dark matter (DM) is one of the main pillars of the current cosmological models to explain structure formation without modifying gravity. Such an introduction induces well documented gravitational effects on structures (Betoule et al. 2014; Ade et al. 2014), however this dominant part of matter continues to elude detection of its constituting particles, whether by direct detection, through accelerators or nuclear recoil experiments (Bernabei et al. 2010; Aalseth et al. 2011; Chatrchyan et al. 2012; Agnese et al. 2014; Aprile et al. 2012, 2022; Zhang et al. 2022; Sirunyan et al. 2021; Tumasyan et al. 2022; Aad et al. 2023), or by indirect searches, through scrutinizing WIMP annihilation detection (Conrad 2014; Armand & Herrmann 2022; Pérez de los Heros 2020), effects on DM stars (Dai & Stojkovic 2009; Kouvaris & Nielsen 2015) or through other indirect effects such as proposed in (Bertolami et al. 2007; Le Delliou et al. 2007, 2015, 2019; Bertolami et al. 2008, 2009, 2012; Abdalla et al. 2009, 2010). Given the uncertainty about the fundamental properties of

DM, experimental and observational efforts must be multifaceted, and many are already probing mass and cross-section regimes relevant for theoretical models (Akerib et al. 2017; Tan et al. 2016; Aprile et al. 2016; Ackermann et al. 2015, see, e.g., the recent reports).

Despite all efforts, to date, every attempt to directly detect DM through laboratory experiments on the Earth have come up empty. Direct detection experiments attempting to observe DM assume it is evenly distributed within each galaxy, however, many theoretical models propose that it may be lumped together in clusters the size of a regular solar system (Berezinsky et al. 2005; Alonso-Álvarez & Jaeckel 2018). At galactic levels, this would not be an issue (for instance, the galaxy rotation curves will remain unchanged), but on smaller scales, it could make a significant difference.

One possibility for this discrepancy is alterations to the basic DM halo model – the potential clumping of DM, which can drastically affect the expected signal. Although astrophysical uncertainties usually have a small influence on the typical direct detection experiments, they are more substantial for annual modulation searches (Green 2017). Clumping of DM would lead to a smaller number of expected interactions, thus reducing the amount of energy

* E-mail: maksym.deliyergiyev@hlrs.de

† E-mail: adel.popolo@oact.inaf.it

‡ E-mail: delliou@lzu.edu.cn

released by DM particles (Berezinsky et al. 2014). The recent experimental estimation of the clumpiness in the current universe assuming the standard cosmological model anchored to the early universe was made in (Hildebrandt et al. 2017; Abbott et al. 2022; Abbott, T. M. C. and others 2023).

This issue welcomes proposals for alternate testing strategies of DM effects. Constraints on DM can be obtained from stars that accrete DM during their lifetime and then collapse into a compact star, or into a black hole (Kouvaris & Tinyakov 2011a; Bertone & Fairbairn 2008; Kouvaris 2008; McDermott et al. 2012; Kouvaris & Tinyakov 2011b; Kouvaris & Nielsen 2015; Kouvaris et al. 2016), inheriting the accumulated DM (Kouvaris & Tinyakov 2011a). Moreover, the cooling process of compact objects can be affected by the capture of DM, which subsequently annihilates (Kouvaris 2008; Bertone & Fairbairn 2008; Kouvaris & Tinyakov 2010; McCullough & Fairbairn 2010; de Lavallaz & Fairbairn 2010; Sedrakian 2019; Bhat & Paul 2020), releasing energy (Pieri et al. 2008). At the same time, self-annihilating DM accreted onto neutron stars (NSs) may change significantly their kinematical properties (Perez-Garcia & Silk 2012) or provide a mechanism to seed compact objects with long-lived lumps of strangelets (Perez-Garcia et al. 2010), in increasingly DM rich environments, should accrete more DM and thus display the characteristic mass decrease, the closer to the galactic centre (Del Popolo et al. 2020b,d,a).

In last years several authors realized that admixing mirror matter with NS matter (Sandin & Ciarcelluti 2009), degenerate DM (Leung et al. 2011), Asymmetric DM (ADM Li et al. 2012; Karkevandi et al. 2022), increasing the ratio of DM to normal matter, the stars had smaller radii and masses. As seen in Ref. (Ciarcelluti & Sandin 2011)'s Fig. 1 for the $M_{DM} - R$ relation, a DM ratio (DM over the total star mass) of the order of 20%, or as shown in Ref. (Goldman et al. 2013) a DM ratio of 50% can give rise to a $2M_\odot$ NS. More refinedly, the precise NS mass depends also on the DM particle mass (Li et al. 2012; Mukhopadhyay & Schaffner-Bielich 2016), so the final NS mass results from a combination of relative acquired DM mass and DM particle mass (Leung et al. 2011). The impact of various DM distribution regimes on observable quantities e.g, the maximum total gravitational mass and the tidal deformability has been considered in (Karkevandi et al. 2022).

In this context, extreme density environments, such as neutron stars (NSs), offer laboratories that can accrete DM. The presence of DM thus strains the NSs saturated neutron Fermi gas. In general, the amount of DM acquired by a given NS follows the determination of the Tolman-Oppenheimer-Volkoff (TOV) equation (Tolman 1939; Oppenheimer & Volkoff 1939, Tolman-Oppenheimer-Volkoff), which governs the amount of DM that can be acquired by a NS, as in e.g., (Tolos et al. 2015; Deliyergiyev et al. 2019). This can produce bounds on candidate DM masses, either directly (Goldman & Nussinov 1989; Kouvaris & Tinyakov 2011b), or after a star that accreted asymmetric DM ends up as NS (Kouvaris & Tinyakov 2011a). Self-annihilating DM produces some characteristic effects on NS (Kouvaris 2008; Bertone & Fairbairn 2008; Kouvaris & Tinyakov 2010; McCullough & Fairbairn 2010; de Lavallaz & Fairbairn 2010; Perez-Garcia & Silk 2012; Perez-Garcia et al. 2010), while non-annihilating DM, among other results (Li et al. 2012; Sandin & Ciarcelluti 2009; Leung et al. 2011; Xiang et al. 2014; Goldman et al. 2013; Tolos et al. 2015), yields the counter-intuitive property of getting smaller (Ciarcelluti & Sandin 2011) and less massive NSs, the more DM they accrete (Sandin & Ciarcelluti 2009; Tolos et al. 2015). Whereas a typical NS has a mass of \approx

$1.4M_\odot$ (de Lavallaz & Fairbairn 2010)¹ in recent years, some pulsars were measured at $2M_\odot$ – PSR J1614-2230 with $M = 1.97 \pm 0.04M_\odot$ (Demorest et al. 2010), PSR J0348+0432 of $M = 2.01 \pm 0.04M_\odot$ (Antoniadis et al. 2013), 4U 1700-37* of $M = 2.44 \pm 0.27M_\odot$ (Zhang et al. 2011), PSR J0952-0607 with $M = 2.35 \pm 0.17M_\odot$ (Romani et al. 2022), and PSR J1748-2021B/NGC 6440B with $M = 2.74 \pm 0.21M_\odot$ (Freire et al. 2008a; Zhang et al. 2011) – larger than the typical observed pulsars. Changing the NS's EoS or adding DM to it can accommodate such large masses. For a stiff EoS, observations vs theory comparison can constrain the EoS and rule out NSs' exotic matter states (e.g., quarks, mesons, hyperons, Schaffner-Bielich 2005). In one of such studies (Ellis et al. 2018) authors compared the result of LIGO/Virgo upper limit to the tidal deformability parameter, Λ , changes for a DM admixed NS, to constrain the EoS. However, the effect of the density dependent DM on the NS properties, such as a tidal deformability and the love number, in a two fluid approach (Das et al. 2022) can be significantly different with respect to the results obtained in a single fluid picture in (Das et al. 2019).

The significant list of quantities responsible for the behaviour of nuclear EoS in the presence of DM was examined in (Panotopoulos & Lopes 2017; Das et al. 2020).

The primary goal of the present work is to stress the idea that NS mass depends on the DM environment. The basic idea dates back to the work of (Del Popolo et al. 2020b,d), which proposed an approximate evolution scheme for the old NS masses with galactocentric distance.

To avoid experimental limitations, such as the limited number of the observed NSs close to the Galactic center, we are trying to check that model (Del Popolo et al. 2020b,d), by assuming that the same dependencies (e.g., the change of density) should be observed inside DM clumps, gearing up with the list of well measured NS masses, and DM clump simulations (Bonnivard et al. 2016a; Charbonnier et al. 2012).

Therefore, we are particularly interested in the possibility of probing the existence and properties of dense dark matter clumps (DMCs) through the detected NSs. Indeed, dense DMCs could form binaries with stars or other dense DMCs within globular cluster (via three-body interaction or dynamical scattering), they could be captured by other binary stars (Bonaca et al. 2018; Wang et al. 2020a), or they may pass in the vicinity of supermassive black holes and give rise to tidal disruption events (Ali-Haïmoud et al. 2016). Dense DMCs with larger densities are likely to survive from tidal interactions with the galactic environment (e.g., see discussion in Aslanyan et al. 2016; Berezinsky et al. 2006, 2013),

but the viable spectra of their mass, density, and radius distribution are still highly uncertain. Along this line, the second aim of this work is to describe an approximate mapping between NSs configurations and DM clumps. The mapping we discuss relies on the similarities between NSs masses and DM clumps scales for the phase-space density distribution describing DM particles.

CLUMPY helps us to simulate any Galactic or extragalactic DM halo including substructures: halo-to-halo concentration scatter, with the several levels of substructures, and triaxiality of the DM halos (Bonnivard et al. 2016a; Charbonnier et al. 2012). This also includes clumps of sub-parsec scales, which are allowed by many

¹ We recall that NSs should have an upper limit $2.01^{+0.04}_{-0.04} - 2.16^{+0.17}_{-0.15}$ Rezzolla et al. (2018), coming from gravitational waves (GW) observations, and a theoretical minimum mass of $0.1 M_\odot$. However, lepton-rich proto neutron stars are unbound below about $1 M_\odot$ Lattimer & Prakash (2004).

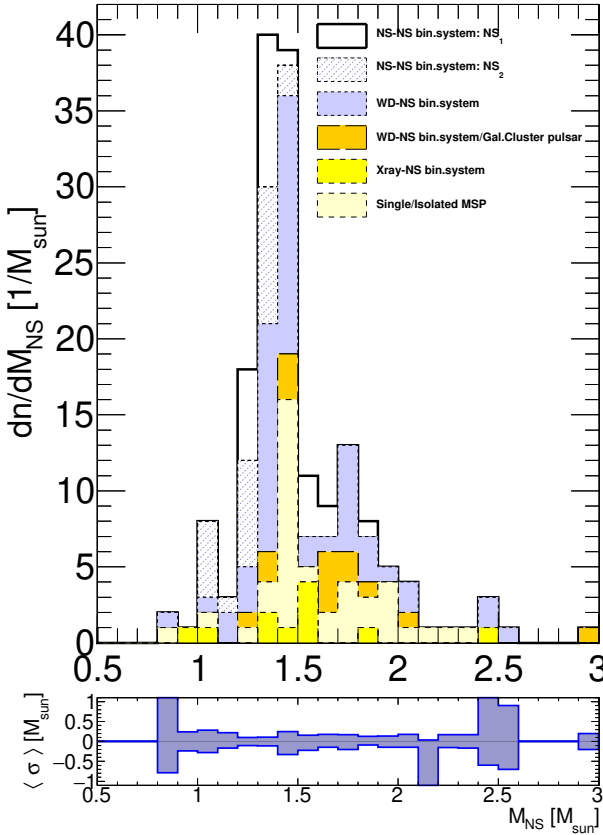


Figure 1. Mass distribution of the examined NSs. Full set includes binary systems such as NS-NS, WD-NS, X-ray-NS, and single Millisecond Pulsars (MSPs). Bottom pad shows the average uncertainty in the NS mass measurements.

DM models as a result of primordial adiabatic isocurvature fluctuations (Kolb & Tkachev 1994), cosmological phase transitions (Schmid et al. 1999), topological defects (Silk & Stebbins 1993), accretion on primordial black holes (PBHs, Bertschinger 1985), etc. Previously CLUMPY has been used to study DM annihilation and/or decay in dSph galaxies (Walker et al. 2011; Charbonnier et al. 2011; Bonnivard et al. 2015, 2016b; Walker et al. 2016) and galaxy clusters (Nezri et al. 2012; Combet et al. 2012; Maurin et al. 2012).

The paper is organized as follows. In Sec. 2, we discuss the NS data used in this study. In Sec. 4, discussed the effects of DM environment on NSs. In Sec. 5, we present our main results on the change of the NSs mass with respect to the DM clumps scale. In Sec. 6 we conclude.

2 DATA USED

In this paper, we use all currently available NS mass measurements summarized in Tables A1 - A2. To find the associated DM clumps we use the Galactic latitude b , longitude l , and the distance estimates for the NS-NS binary systems, NSs in X-ray binaries, radio millisecond pulsars (MSPs), White Dwarfs-Neutron stars (WDs-NSs) systems, WDs-NSs Galactic Cluster pulsar. The mass distribution of the examined NSs is shown in Fig. 1, where different color denote contributions from each of the considered star systems. The distribution includes NSs-NSs binary systems (black and dashed histogram),

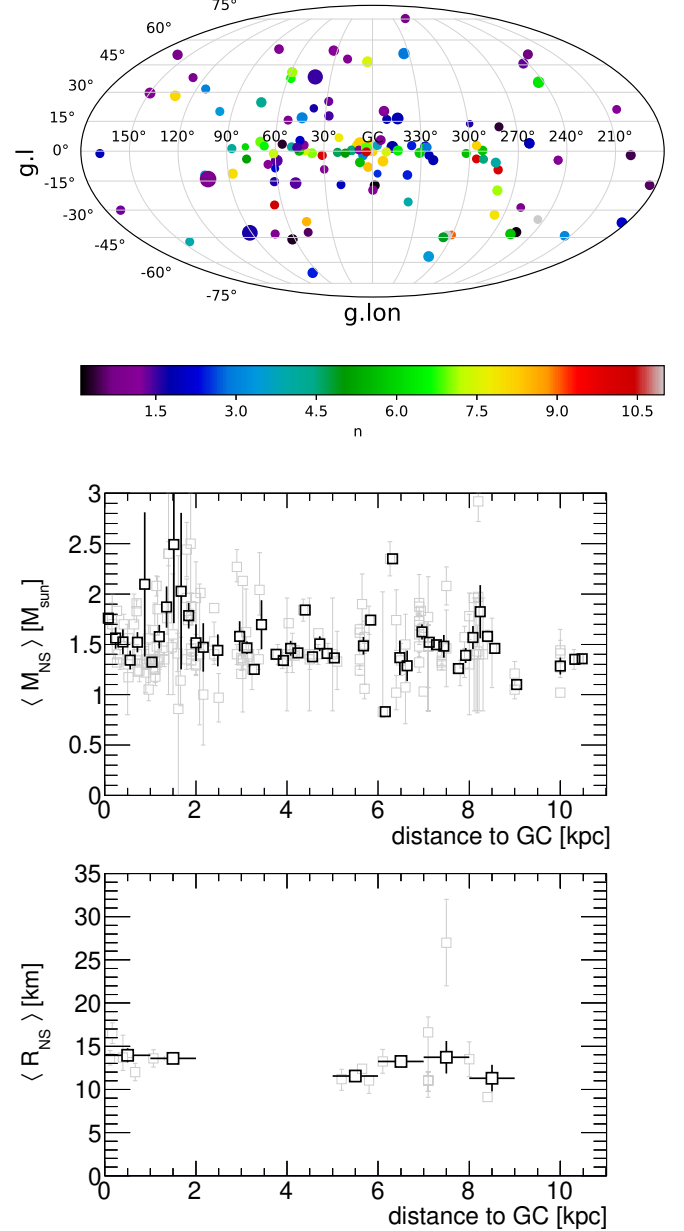


Figure 2. Top: Sky map of the examined NS with the color coded distances, while the NS masses are encoded in the scale of the circles. Center: Mass distribution of the examined NSs as a function of the distance to Galactic centre. Bottom: Radius distribution of the examined NSs as a function of the distance to Galactic centre. Black boxes - the average mass and radius, the vertical error bars simply reflect the statistical uncertainty at the given bin; light grey boxes - the measured masses and radii of the NSs with the measured uncertainties, see Tables A1-A2.

WDs-NSss binary systems (blue histogram), WDs-NSs binary systems/Galactic cluster pulsars (orange histogram), X-ray-NSs binary systems (yellow histogram), single/isolated MSPs (light yellow histogram). The bottom panel in Fig. 1 shows the average uncertainty in the NSs mass measurements in the given bin.

Fig. 2 (top) is a sky map of the examined NS with the color coded distances, while the size of the circle markers represents the NSs masses. The bottom panel describes the average mass distribution of the NSs as a function of the distance from the Galactic center.

3 DARK MATTER CLUMPS SIMULATION

Many studies (Berezinsky et al. 2003; Ricotti & Gould 2009; Scott & Sivertsson 2009; Berezinsky et al. 2013; Bringmann et al. 2012; Berezinsky et al. 2014) pointed out that the DM distribution into a halo is not homogeneous, and superdense dark matter clumps (SDMC) (i.e. bounded DM objects are virialized at the radiation dominated era), and ultra compact minihaloes (UCMH) formed from secondary accretion on SDCMs (Berezinsky et al. 2013), are present in the halo.

In literature are often encountered terms like "minihaloes", and "microhaloes", stressing the similitudes, when neglecting gas dynamics, between these DM objects and the DM haloes in which galaxies are found. Superdense clumps are formed by self-gravitating perturbed regions at the equivalence time, t_{eq} , while objects formed at $t > t_{\text{eq}}$ have lower densities, and are dubbed "clumps" (Berezinsky et al. 2014). The clumps have a mass spectrum (Berezinsky et al. 2014) characterized by a minimum mass, M_{min} depending on the DM particle considered, and produced by the diffusion of DM out of the perturbation, and the following free streaming. In the case of neutralino, $10^{-11} M_{\odot} < M_{\text{min}} < 10^{-3} M_{\odot}$ (e.g., (Bringmann 2009)).

The characteristics of SDMC, and UCMH have been studied by means of simulations e.g. (Ricotti & Gould 2009), or analytical models (Berezinsky et al. 2013, 2014). In this paper, we rely on the CLUMPY simulations which were used to quantify DM clump masses and scales in the vicinity of known NSs, assuming 100 and 500 GeV DM particle mass. We refer the reader to (Charbonnier et al. 2012; Bonnivard et al. 2016a) for an extensive description of the CLUMPY code features and validation, while here we briefly summarize the most important features for our analysis.

CLUMPY mostly has been used to calculate the J -factor

$$\begin{aligned} J(\vec{k}, \Delta\Omega) &= \int_{\Delta\Omega} \int_{\text{l.o.s.}} \rho_{\text{dm}}^2 dl d\Omega \\ &= \int_0^{2\pi} \int_0^{\theta_{\text{int}}} \int_{\text{l.o.s.}} \rho_{\text{dm}}^2(\vec{k}; l, \theta, \phi) \sin\theta dl d\theta d\phi. \end{aligned} \quad (1)$$

Here, we used the latest CLUMPY release, which includes additional outputs, that provides a better description of several quantities related to DM haloes and their substructures, which is our main interest. For this work, we mainly use CLUMPY in the so-called ‘skymap mode’² which allows the fast computation of full-sky maps of DM annihilation or decay signals. In CLUMPY, the DM density ρ_{dm} is integrated along the line of sight (l.o.s.), and up to a maximum angular distance θ_{int} . The overall DM density can be written $\rho_{\text{tot}} = \rho_{\text{sm}} + \rho_{\text{subs}}$, where ρ_{sm} corresponds to the smooth component, and ρ_{subs} corresponds to the substructures of the Galactic DM halo. The galaxies with different DM clumps configurations which were used in this analysis were simulated using smoothing of the output J -factor skymaps with a Gaussian beam and calculating the angular power spectrum of the maps. The full width at half maximum of Gaussian smoothing was set to 0.8.

We analyze galaxies from $z = 0$, which should correspond to the characteristic overdensity value of $\Delta = 200$. At this period of time, the galaxy should already change from being a very clumpy, gas-rich system that forms stars vigorously to a more regular and moderately star-forming galaxy.

As an illustrative example, we provide 2D-skymap plots for the Milky-Way DM haloes in Fig. 3 (left). In this example, the total

density profile of the halo is parameterized by an Einasto profile with $r_{-2} = 15.14$ kpc, $\alpha_E = 0.17$ (Fornasa et al. 2013) and a local DM density of $\rho = 0.4 \text{ GeV cm}^{-3}$ at $R = 8.0$ kpc. All our Galaxy simulations use a virial radius of DM halo $r_{\text{vir}} = 260$ kpc, yielding a total MW mass $M_{\text{MW}} = 1.1 \times 10^{12} M_{\odot}$, in agreement with (Nesti & Salucci 2013), while DM clumps mass range is $10^6 - 10^{10} M_{\odot}$. Fig. 3 (left) shows the color scale for the J -factor values per steradian in case of DM annihilation (Bonnivard et al. 2016a). In Fig. 3(right) we show 746 extracted clumps from the sky map on the left with masses greater than $10^7 M_{\odot}$, where the clumps location has 5% Gaussian smearing, the color indicates their spatial concentration.

CLUMPY provides us with a multidimensional criterion for the definition of clumps that helps us more easily to select them in association with the NSs. This criterion includes parameters, such as, the clump Δ -scale, R_{Δ} , the tidal and mass scales R_{tidal} , and M_{tidal} respectively, and the clump masses M_{Δ} , their galactic coordinates, distances, the critical DM density ρ_s , and the scale radius r_s at that point.

Whether substructures in subhalos are scaled-down versions of substructure in main halos remains an open question (Springel et al. 2008). Using CLUMPY we only consider one level of substructure within the halo under scrutiny (Galactic halo or individual halo such as a dwarf spheroidal galaxy), and the properties of these sub-halos can be independently chosen from that of the parent halo.

To date, there is no consensus as to what the Galactic DM profile, $\rho_{\text{dm}}(r)$, should be. There is some dynamical evidence that the Galactic DM halo might be triaxial (Law et al. 2009) and numerical simulations, such as the Aquarius (Springel et al. 2008) or the Via Lactea runs (Diemand et al. 2008) also find non-spherical halos. All clumps have the same inner DM distribution, which in our case is an Einasto profile. The mass of the clump generally suffices to determine all its properties, i.e., its size $R_{\text{vir}}^{\text{cl}}$, and once an inner density profile is chosen, its scale radius r_s and scale density ρ_s . Parametrizations of the mass-concentration relation have been established from numerical simulations for isolated field halos (Bullock et al. 2001; Eke et al. 2001) but the concentration generally presents a significant scatter (Wechsler et al. 2002). We used Moline’s (Moliné et al. 2017) mass-concentration model of subclump.

A critical distance l_{crit} for the clumps in the Galaxy gives $\langle n_{\text{cl}} \rangle$, the average number of clumps, obtained from a Poisson distribution of mean value $\langle n_{\text{cl}} \rangle$.

Assuming that N_{tot} is the total number of clumps in a DM host halo, then the overall distribution of clumps is written as:

$$\frac{d^2 N}{dV dM} = N_{\text{tot}} \frac{d\mathcal{P}_V(r)}{dV} \frac{d\mathcal{P}_M(M)}{dM}, \quad (2)$$

where the spatial and mass distribution are probabilities, respectively normalised as:

$$\int_V \frac{d\mathcal{P}_V(r)}{dV} dV = 1, \text{ and } \int_{M_{\text{min}}}^{M_{\text{max}}} \frac{d\mathcal{P}_M(M)}{dM} dM = 1. \quad (3)$$

Analysis of N-body simulations have shown the mass distribution to vary as a simple power law

$$\frac{d\mathcal{P}_M(M)}{dM} \propto M^{-\alpha_M} \quad (4)$$

with $\alpha_M \approx 1.9$.

Given the mass and spatial distribution, the total number of clumps N_{tot} can be determined as following:

$$N_{\text{tot}} = \frac{f_{\text{cl}} M_{\text{tot}}}{\langle M_{\text{1cl}} \rangle} \quad (5)$$

with $\langle M_{\text{1cl}} \rangle$ the average mass of one DM clump, and the mass fraction f_{cl} of clumps.

² Simulation for the whole Galactic latitude and longitude ranges.

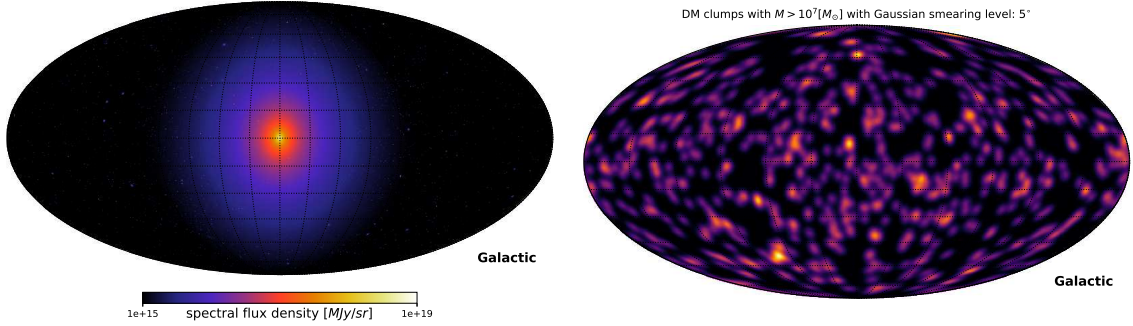


Figure 3. Left: Differential intensity skymap for an observer located at $R = 8.0$ kpc looking towards the centre of the galactic halo for γ -rays from annihilation at 4 GeV for $m_\chi = 100$ GeV and $\chi\chi \rightarrow b\bar{b}$ channel. The skymap is drawn in the -g8 mode of CLUMPY (Bonnivard et al. 2016a; Charbonnier et al. 2012) for a numeric resolution of $N_{\text{side}} = 2048$ (corresponding to a pixel diameter of $\theta_{\text{pix}} = \Omega^{1/2} = 1.^{\circ}72$) with the parameters for a spherically symmetric halo specified in the text. The initial random seed is 1332. The colour scale gives the J -factor values per steradian in case of DM annihilation (Bonnivard et al. 2016a). Right: Extracted from the map on the left DM clumps with masses greater than $10^7 M_\odot$. A total number of 746 clumps is plotted with the Gaussian smearing of 5%.

From the spatial distribution $d\mathcal{P}_V(r)/dV$ one can define the average clump density ρ_{subs} as

$$\langle \rho_{\text{subs}(r)} \rangle = f_{\text{cl}} M_{\text{tot}} \frac{d\mathcal{P}_V(r)}{dV} \quad (6)$$

We assume the standard Λ cold dark matter (Λ CDM) cosmology with the *WMAP5* cosmological parameters, namely $\Omega_m = 0.27$, $\Omega_\Lambda = 0.73$, $\Omega_b = 0.045$, $h = 0.7$ and $\sigma_8 = 0.82$ (Ullio et al. 2002; Komatsu 2003; Komatsu et al. 2009; Moliné et al. 2017). Each halo was selected to have a given virial mass at $z = 1$ and no ongoing major merger at that time. This latter criterion eliminates less than 10% of the haloes, which tend to be in dense protocluster environments at $z \sim 1$. The target virial masses at $z = 0$ were selected in the range $M_{\text{vir}} = 10^6 - 10^{10} M_\odot$.

Generating skymaps with CLUMPY starts from setting DM properties: smooth DM profile, spatial and mass distribution of Galactic substructures, halo mass-concentration relation, DM particle mass, and annihilation/decay channels. The computation has been optimized to draw only subhalos that outshine the mean DM signal (set by a user-defined precision), leading to a decomposition of the substructure signal $J_{\text{subs}}^{\text{tot}} = J_{\text{drawn}} + \langle J_{\text{subs}} \rangle$ into two components: J_{drawn} is the signal from the substructures drawn in a realization of the skymaps, and $\langle J_{\text{subs}} \rangle$ is the average signal from all ‘unresolved’ halos³, i.e., faint subhalos whose intrinsic J -factors do not pass the threshold defined from the precision level required by the user. Additional levels of clustering within subhalos are also considered using this average description.

To assess sensitivity prospects between NSs and DM clumps, we explore various parameter sets for the substructure density, while the average total Galactic halo density is left unchanged. We build sets of models by varying seven important properties of Galactic substructures such as the mass distribution, Eq.(4), the power law index α_M , the width of the mass-concentration distribution σ_c , the number of halos N_{calib} between $10^6 - 10^{10} M_\odot$ (this number is used as a calibration for the total number of subhalos). We choose $N_{\text{calib}} = 150$ as our default value. For more subhalo-rich configurations, we used $N_{\text{calib}} = 200 - 300$ as motivated by the results of DM-only simulations (Springel et al. 2008).

³ For legibility purpose, we define $\langle J_{\text{subs}} \rangle$ to be the sum of $\langle J_{\text{subs}} \rangle$ and $J_{\text{cross-prod}}$ as defined in (Bonnivard et al. 2016a)

4 NEUTRON STARS IN THE DARK MATTER ENVIRONMENT

The accumulation of DM, studied by several authors (Kouvaris & Tinyakov 2010; de Lavallaz & Fairbairn 2010; Yang & Gao 2011; Kouvaris & Tinyakov 2011a; Zheng & Chen 2016), happens in several phases (Güver et al. 2014). In the first one, the ambient DM is captured by the NS, when DM scatters with nucleons. In the second phase, scattering of DM with neutrons produces a decrease in the DM particle orbit radius. In the third phase, DM interacts with the already captured DM. DM thermalization with neutrons gives rise to the possibility to form a Bose-Einstein condensate, and DM becomes self-gravitating collapsing and forming a black hole (Güver et al. 2014; Kouvaris 2013). The evolution of the DM number, N_{dm} , is given by

$$\frac{dN_{\text{dm}}}{dt} = C_c + C_s N_{\text{dm}} \quad (7)$$

(Güver et al. 2014), where C_c is the capture rate due to DM-nucleon interaction, and C_s is the capture rate due to DM self-interactions (Güver et al. 2014), given by

$$C_s = \sqrt{\frac{3}{2}} \frac{\rho_{\text{dm}}}{m_{\text{dm}}} (\sigma_{\text{dm}}^{\text{elas}} v_{\text{esc}}(R)) \frac{v_{\text{esc}}(R)}{\vec{v}} \langle \hat{\phi}_{\text{dm}} \rangle \frac{\text{erf}(\eta)}{\eta} \frac{1}{1 - \frac{2GM}{R}}, \quad (8)$$

where $v_{\text{esc}}(R)$ is the escape velocity from the surface of the NS, $\sigma_{\text{dm}}^{\text{elas}}$ is the DM elastic scattering cross-section, m_{dm} is the mass of the DM particles, $\hat{\phi}_{\text{dm}}$ is a dimensionless potential, which embodies the compactness of the star, the parameter $\eta^2 \equiv 3/2(v_{NS}/\vec{v})^2$ depends on the velocity, v_{NS} , of the NS in the Galaxy.

Following (Kouvaris & Tinyakov 2010, 2011a; de Lavallaz & Fairbairn 2010; Zheng & Huang 2011; Fan et al. 2012), we will neglect the accretion due to self-interaction.

To calculate C_c (Kouvaris 2008), we assumed a Maxwellian DM distribution. Then, were calculated the DM orbits that intersect the NS’s, and then the subsample of those losing enough energy to be

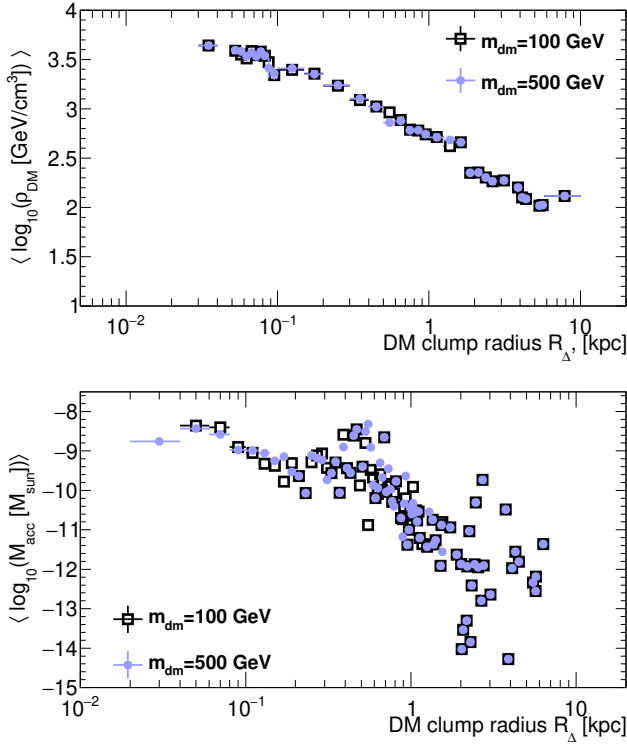


Figure 4. Top: DM density distribution in a minihalo/clump. Bottom: Accreted DM mass in a minihalo/clump, computed with the help of Eq.(11), where DM density distribution in a minihalo/clump, was computed from the Einasto profile using the ρ_s and r_s values for the selected clump associated to the NS taken from CLUMPY simulation. The results are shown for galaxy models assuming $m_{\text{dm}} = 100$ and 500 GeV . We used only those clumps that are associated with the NS.

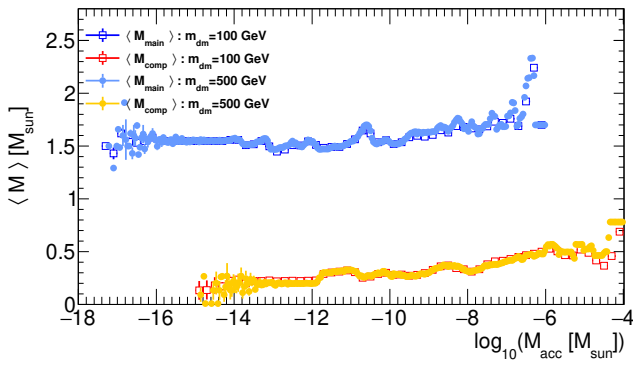


Figure 5. Change of the average star (NS/WD) mass with respect to the DM mass accreted inside the selected clumps, where the accreted mass was computed with the help of Eq.(11). Results for the clumps obtained assuming particle mass $m_{\text{dm}} = 100 \text{ GeV}$ (box) and 500 GeV (circles). The profiles are shown for the main star (azure, blue) and companion star separately (red, orange).

captured. The accretion rate can be written as

$$\begin{aligned} C_c &= \frac{8\pi^2}{3} \frac{\rho_{\text{dm}}}{m_{\text{dm}}} \left(\frac{3}{2\pi\bar{v}^2} \right)^{3/2} GMR\bar{v}^2 \left(1 - e^{-3E_0/\bar{v}^2} \right) \xi f \\ &= 1.1 \times 10^{27} \text{ s}^{-1} \left(\frac{\rho_{\text{dm}}}{0.3 \text{ GeV cm}^3} \right) \left(\frac{220 \text{ km}}{v} \right) \left(\frac{\text{TeV}}{m_{\text{dm}}} \right) \\ &\quad \left(\frac{M}{M_{\odot}} \right) \left(\frac{R}{R_{\odot}} \right) \left(1 - e^{-3E_0/\bar{v}^2} \right) f \end{aligned} \quad (9)$$

(Kouvaris & Tinyakov 2011a; Güver et al. 2014), where ρ_{dm} is the local DM density, \bar{v} is the average DM velocity in the Galactic halo (Kouvaris & Tinyakov 2010), ξ is the Pauli blocking factor defined in (Güver et al. 2014; Bell et al. 2020). M , and R the mass and radius of the star, E_0 is the DM maximum energy per DM mass, which can give rise to capture, and $E_0 \gg 1/3\bar{v}^2$, implying $e^{-3E_0/\bar{v}^2} \approx 0$. f is the fraction of particles undergoing scatterings in the star, and $f = 1$ for $\sigma_{\text{dm}} > 10^{-45} \text{ cm}^2$, or $f = 0.45\sigma_{\text{dm}}/\sigma_{\text{crit}}$, and $\sigma_{\text{crit}} \approx 6 \times 10^{-46} \text{ cm}^2$.

The capture rate of fermionic DM scattering from neutrons within a NS in the zero temperature approximation can be written as following

$$\begin{aligned} C_c &\approx \frac{4\pi}{v_{NS}} \frac{\rho_{\text{dm}}}{m_{\text{dm}}} \text{Erf} \left(\sqrt{\frac{3}{2}} \frac{v_{NS}}{v_d} \right) \\ &\quad \times \int_0^{R_{NS}} r^2 dr n_n(r) \frac{1 - B(r)}{B(r)} \langle \sigma_{\text{dm}}(r) \rangle, \end{aligned} \quad (10)$$

where $(1 - B(r))$ plays the role of the escape velocity $v_{esc}^2(r)$ and $1/B(r)$ provides a relativistic correction, v_{NS} is the NS velocity and v_d is the DM velocity dispersion, while $n_n(r)$ is the neutron number density (Bell et al. 2020). This approximation is valid for the intermediate DM mass range.

The capture rate has been estimated by several other authors (Kouvaris 2013; Fan et al. 2012; Zheng & Chen 2016; Güver et al. 2014) and the results are more or less in agreement with that of (Kouvaris & Tinyakov 2011a).

In the case of a typical NS, with a simple transformation of Eq.(9) one may get the following expression for the accreted total mass:

$$M_{\text{acc}} = 9.29 \times 10^{41} \left(\frac{M}{M_{\odot}} \right) \left(\frac{R}{R_{\odot}} \right) \left(\frac{\rho_{\text{dm}}}{0.3 \text{ GeV cm}^3} \right) \left(\frac{t}{\text{Gyr}} \right) f \text{ GeV}, \quad (11)$$

which gives $\approx 10^{-14} (10^{-11}) M_{\odot}$, for the DM trapped in a NS (WD). In Fig. 4, we present two key aspects of our analysis. First, we display the average clump density, equation (6), as a function of clump radius. Second, we show the accreted DM mass within clumps. This mass is calculated using equation (11) and is based on the DM density distribution within these structures, determined from the Einasto profile with ρ_s and r_s values specific to the selected clumps associated with NS, derived from the CLUMPY simulation.

The previous equation is an underestimate of the accreted mass since it does not take into account the accretion by the NS progenitor, which is of the same order as that acquired in the NS phase (Kouvaris & Tinyakov 2010), or the accretion due to DM self-interaction (Güver et al. 2014).

The maximum density in the center of clumps can be estimated by means of the annihilation criterion, and gives

$$\rho(r_{\min}) \approx \frac{m_{\text{dm}}}{\langle \sigma v \rangle (t_0 - t_f)}, \quad (12)$$

where t_0 is the present time (13.7 Gyr), t_f the formation time (59 Myr (0.49 Gyr) for non-contracted (contracted) UCMHs (Scott & Sivertsson 2009)), $\langle \sigma v \rangle \approx 3 \times 10^{-26} \text{ cm}^3/\text{s}$ the thermal

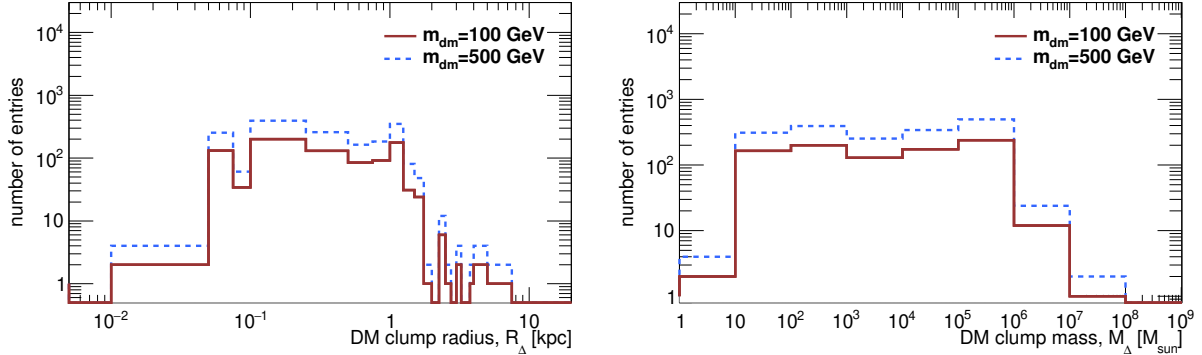


Figure 6. (left): The outer bound of the DM-clumps in the vicinity of the examined. (right): The mass of the DM clumps in the vicinity of the examined NSs in absolute units. The real-space distance between NSs and DM clumps coordinates should be less than 0.01, 0.05, 0.1, 0.25, 0.5, 0.75, 1, 2, and 5 kpc, while the scale of the selected clumps should be greater than the distance.

cross section, and m_{dm} the DM particle mass. For a 100 GeV particle, Eq. (12) gives $\rho(r_{\min}) = 7.7 \times 10^9 \text{ GeV/cm}^3$, namely $\approx 2.6 \times 10^{10}$ larger than the local DM density, implying that a NS would acquire a DM mass equal to $\approx 7.5 \times 10^{-4} M_{\odot}$.

5 RESULTS

For this analysis we simulated 19 galaxies⁴ with the help of CLUMPY (Bonnivard et al. 2016a; Charbonnier et al. 2012) with the numerical resolution of $N_{\text{side}} = 2048$ (corresponding to a pixel diameter of $\theta_{\text{pix}} = \Omega^{1/2} = 1.^{\circ}72$) with the parameters for both spherically symmetric and triaxial rotated halos. To compute fluxes for annihilation and decay, the tabulated DM γ -ray and ν spectra from (Cirelli et al. 2011) were used for $m_{\text{dm}} = 100$ and 500 GeV, forced to decay only via $\chi\chi \rightarrow b\bar{b}$ channel⁵. Since we are interested only in the location of the DM clumps, their mass and scale characteristics, the particular decay channel selection or their mixture was not relevant to our analysis.

The spatial distribution of subhaloes dP_V/dV is described by the Gao profile (Gao et al. 2004; Madau et al. 2008). The mass distribution dP_M/dM follows a power-law with index $\alpha_M = 1.9$, normalized by an abundance of 150–300 subhaloes in the mass range $10^6 - 10^{10} M_{\odot}$.

To address the main aim of our research we examined all currently measured NSs in single and binary systems⁶, which are listed in the Tables A1–A2.

Our analysis is based on the simplest approach, we select any massive object – DM clump in the vicinity of the NS. The real separation distance between NS and clump should be less than 0.1 kpc (0.05 kpc for a finer, more computationally expensive check run, however yielding insufficient statistics), while the delta radius, R_{Δ} , and tidal radius, R_{tidal} , of such a clump, should be greater than this distance cut. For the spherical over density we use M_{Δ} and R_{Δ} , for the tidal over density – M_{tidal} and R_{tidal} . Once the clump matches our

⁴ For such high resolutions, the smoothing via spherical harmonics – as done by the implementation in CLUMPY – is very computationally expensive. This is why the number of galaxies in our analysis is small.

⁵ Default decay channel in CLUMPY.

⁶ We collect 146 neutron stars with the measured masses, coordinates, and distances. We are aware that some NSs masses in our list were not exactly measured but were assumed to compute the companion star mass, such as (Ng et al. 2015; Cameron et al. 2020).

selection criteria, we explore dependencies between the parameters of this clump and NSs localized in this clump.

By using Eq.(11), we computed the accreted DM mass for the examined NSs using the local density ρ_{dm} , the scale density, ρ_s , and radius, r_s , for the selected clumps. In addition, we have to assume the formation age of 13.7 Gyr, a typical radius of 10 km, for NSs, and 7000 km, for the companion WDs, respectively, for the stars whose age is not measured yet, see Tables A1 – A2. In Fig. 5 we show the results of such computation for the main star (NS) and companion WD.

We see that at the range of $10^{-14} - 10^{-8} M_{\odot}$ of M_{acc} there is no mass change for both types of stars. However, once the accreted mass goes beyond $10^{-8} M_{\odot}$ the NSs mass tends to exponentially increase, while the WDs follow the same tendency but in a linear manner. This is in line with the results presented in (Deliyergiyev et al. 2019) if one assumes that DM interaction strength with ordinary matter is strong and of order 10^3 .

To proceed we need to understand the morphology of the selected clumps. In Fig. 6, we plot the scale (left panel) and mass (right panel) distributions for the clumps associated with the NSs, namely the candidates' clumps that enclose one or more of the NSs, requiring that the real-space distance between the NSs and clumps coordinates should be less than 0.01, 0.05, 0.1, 0.25, 0.5, 0.75, 1, 2 and 5 kpc, respectively, while the radius of the selected clump must be greater than this distance. This assures us that at least one NS is located inside the clump. We see that, after analyzing all modeled galaxies, the bulk of the clump scale distribution is localized in the range of 0.1 to 3 kpc, while the mass is distributed in the range of 10 to $10^7 M_{\odot}$.

The numbers of the clumps associated to one given NS are shown in Fig. 7. We show these clump multiplicities for two different selection categories, when the real space separation distance between DM clumps and NSs coordinates should be less than 1 kpc, while the clump radius is greater than 1 kpc (left panel), and when the real space separation distance between DM clumps and NSs coordinates should be less than 0.05 kpc, while the clump radius is greater than 0.05 kpc (right panel). At the distance of 0.01 kpc, only 2 clumps out of all simulated galaxies matched our selection criteria.

The results of this selection analysis are interpreted by mapping DM clumps on the sky map. Inclusion contours of the DM clumps are presented in Fig. 8, where we show the distributions of DM clumps into different categories based on their mass (top) and outer bound radius (bottom), as seen projected on the sky in Galactic

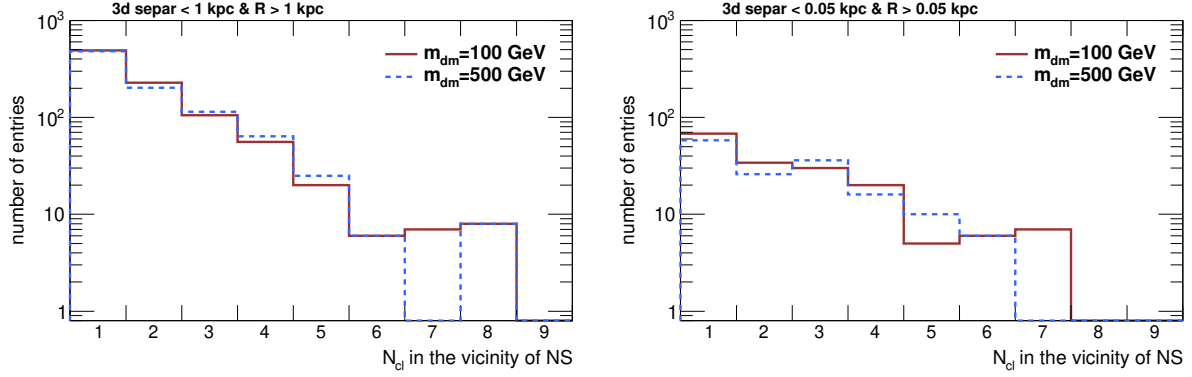


Figure 7. The number of DM clumps in the vicinity of the examined NSs in absolute units. (left): The multiplicity of DM clumps in the vicinity of the NSs when the real space separation distance between DM clumps and NSs coordinates should be less than 1 kpc, while the scale of the selected clumps should be greater than 1 kpc. (right): The distance between NSs and DM clumps coordinates should be less than 0.05 kpc, while the scale should be greater than 0.05 kpc.

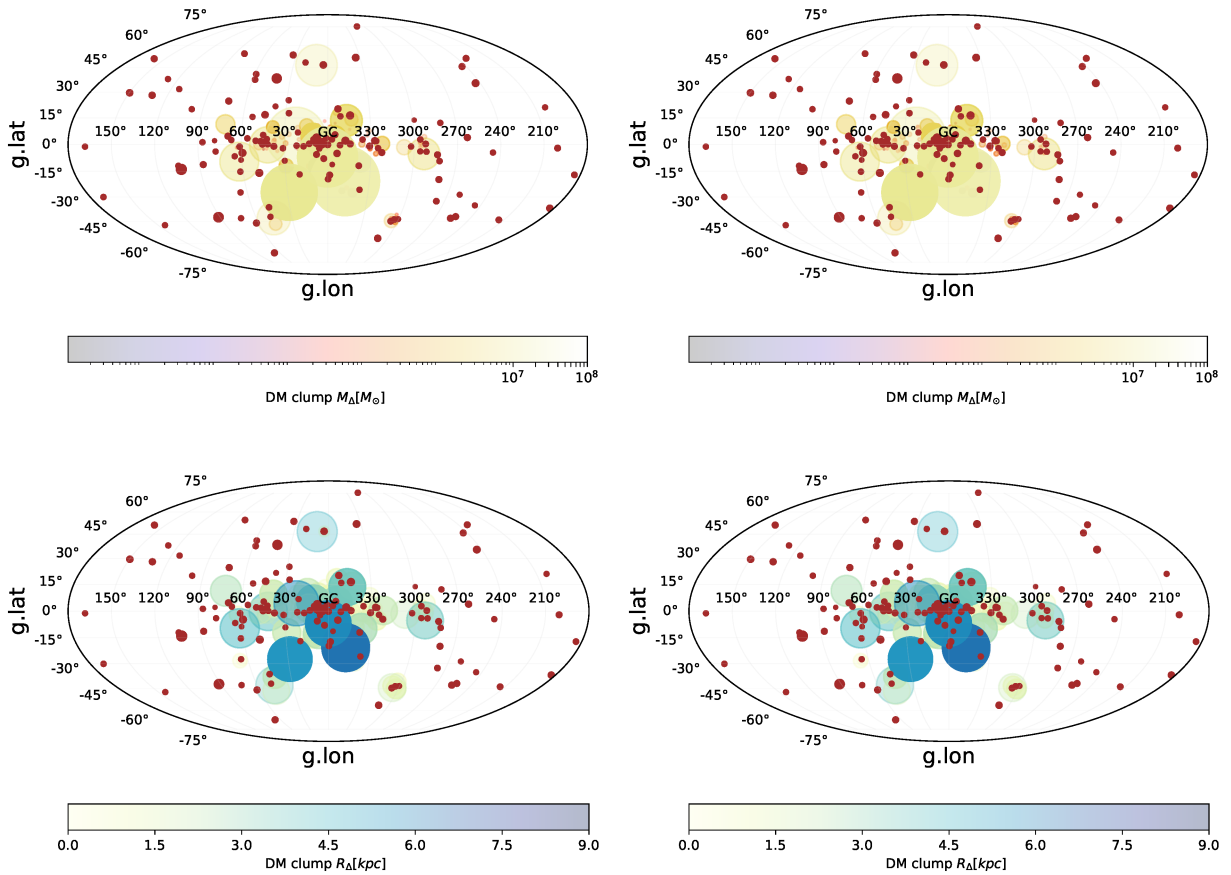


Figure 8. The distribution of DM clumps mass (top) and outer bound radius (bottom), as seen projected on the sky in Galactic coordinates. DM clumps were selected with respect to the 3d-distance and scale. Namely, the 3d-separation distance should be less than 0.05 kpc, and the radius of the selected clump should be greater than 0.05 kpc. The circle size indicates the mass of the DM clump (top), and the scale of the DM clumps (bottom). Red data points indicate known NSs. (left) CLUMPY simulation using $m_{dm} = 100$ GeV; (right) $m_{dm} = 500$ GeV.

coordinates. The scale of circles denotes the distance of these clumps to the Galactic center, while color denotes the mass (top) and radius (bottom). The red circles indicate NSs that were examined in this paper. The results of the analysis can then be used to infer properties of the underlying DM distribution, such as its spatial distribution, density, and velocity. The selected clumps are mostly located in the

region of sky within Galactic longitude $60^\circ < l < 300^\circ$ and latitude $|b| < 45^\circ$, see Figs.8. On the one hand, we see that some NSs could theoretically interact or be wrapped up with/by more than one clump, see Fig.7. The simulations with CLUMPY show us that 2-3 clumps with a radius of 0.1 kpc may wrap a single NS within the separation distance of 0.01 kpc. Also, we note, that one clump may

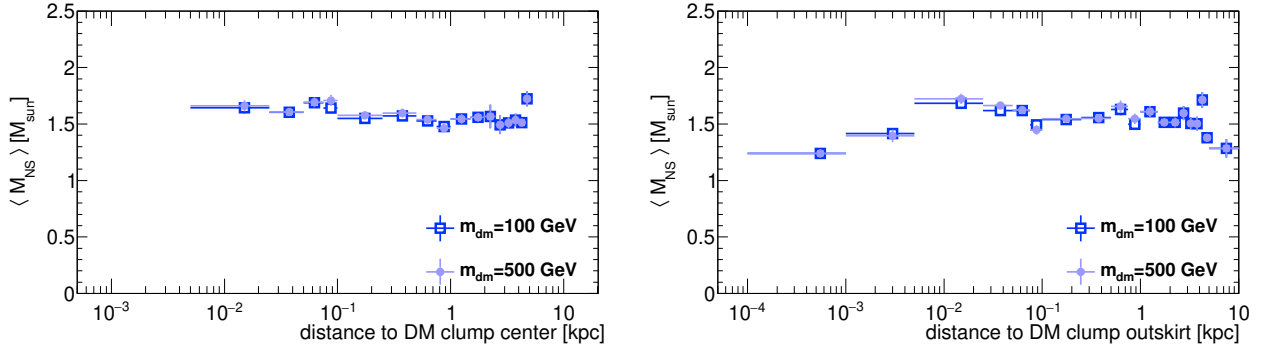


Figure 9. Left: The distribution of NS mass inside the DM clumps as function of distance to the clump center. Right: The distribution of NS mass inside the DM clumps as function of distance to the clump outskirt. Results are shown for the DM clumps produced with the help of CLUMPY assuming $m_{\text{md}} = 100 \text{ GeV}$ (boxes); $m_{\text{md}} = 500 \text{ GeV}$ (circles).

wrap up more than one NS, as seen from Fig. 8. On the other hand, there is a number of NSs for which we did not manage to find an associated DM clump among simulated galaxies even in the vicinity of 6 kpc, that will have a radius greater than 6 kpc.

Due to the inhomogeneity of the DM distribution in the galactic halo, one should expect that NSs and WDs forming in DM clumps have a different structure than those forming outside of them. This is because, in clumps, the DM density is larger than in the environment, and increases going toward the center of the clump. This implies a larger accretion of DM by NSs, and consequently, since larger content of DM in those objects implies a smaller mass (Deliyergiyev et al. 2019; Del Popolo et al. 2020c).

To determine how the NS mass change inside the clump obtained with the help of CLUMPY, the data analysis was performed in several steps. First, we plot the NSs mass distribution as a function of the distance to the center of the selected clump, Fig. 9(left). We see that it is almost constant, while in the close distance range to the DM clump outbound/outskirt (Fig. 9 right) the NS mass behaves differently. It decreases close to the DM clump outbound/outskirt, then in the range of distances from 0.01 to 1 kpc it is flat, and beyond 2 kpc it starts to bend down to small masses.

Second, a fit to the star mass is performed with the main NS mass and total mass of the binary systems, split into the merged and differential selection categories with respect to the DM clump radius. The resulting observed tendency in the merged categories is shown in Fig. 10 for R_{Δ} and R_{tidal} separately, while the results for the differential categories are shown in Fig. 11.

More in detail, Fig. 10 shows the mass of NSs change with the clump scale in the case of DM particle mass 100 GeV and 500 GeV. The top panel of Fig. 10 shows the NSs mass as a function of the clump radius, R_{Δ} , with the 95%, and 68% confidence bands, and for 100 GeV (left panel), and 500 GeV, (right panel). The bottom panels represent the same quantity for the tidal radius, R_{tidal} . Clumps were selected in the vicinity of 0.01, 0.05, 0.1, 0.25, 0.5, 0.75, 1, 2, and 5 kpc to the NSs, and the clump scale was requested to be larger than this separation distance. We merged statistics from all clumps we found in the vicinity of 0.01, 0.05, 0.1, 0.25, 0.5, 0.75, 1, 2, and 5 kpc. In Fig. 10 (top), one may notice some transition region between very small clumps ($10^{-2} - 10^{-1}$ kpc) and clumps with a radius greater than 10^{-1} kpc. We assume that such artifacts might be driven by the CLUMPY clump modeling.

In Fig. 11, we plot the total mass of the binary systems as a function of the clump radius. The plot was built in a similar way to Fig. 10, and again, we observe a decrease of the mass towards the outskirts

of the clump. In other terms, the plots show that the NSs have a mass decreasing towards the outskirts of the clump, namely the opposite of what is predicted by (Del Popolo et al. 2020b), assuming that DM interaction strength with the ordinary matter is low.

However, we do not see this as a discrepancy (Del Popolo et al. 2020b) and our results. In (Del Popolo et al. 2020b) NS mass was shown as a function of distance, while Figs. 10 - 11 show the NS mass as a function of the clump scale.

6 CONCLUSIONS AND DISCUSSIONS

In this paper, we checked the prediction of (Del Popolo et al. 2020b), namely that the neutron stars (NSs) mass decreases with the increasing accumulation of dark matter (DM), and consequently, in our galaxy, the NSs mass decreases going toward the galactic center. The predictions made in (Del Popolo et al. 2020b) were based on the distribution of DM in our galaxy, characterized by an increase going towards the galactic center. Changes in the NSs structure and decrease in their mass when getting closer to the galactic center was only produced in the very vicinity to that galactic center. Unfortunately, nowadays, we do not have enough information on NSs close to the galactic center. To verify our prediction, we then turned to DM clumps contained in the galaxy. These objects are characterized by an increase of the density towards their center, their density reaching similar values to that in the vicinity of the galactic center.

We then used the known NSs located in DM clumps. To check the quoted predictions, and to generate the clumps, we used CLUMPY simulations of any Galactic or extragalactic DM halo including substructures: halo-to-halo concentration scatter, with several levels of substructures, and triaxiality of the DM halos (Bonnivard et al. 2016a; Charbonnier et al. 2012). The mass range of the DM clumps that we found in the vicinity of the neutron stars is $10 < M_{\text{clump}} < 10^8 M_{\odot}$, while the scale of these clumps is $10^{-3} < R_{\text{clump}} < 10$ kpc. We studied how the mass of NSs changes in the quoted clumps, showing that the NSs mass is almost stable going towards the outskirts of the DM clumps. This result is in agreement with (Del Popolo et al. 2020b) taking into account that at distances greater than 0.01 kpc from the clump center, the NSs are much closer to the outskirt of selected DM clump. Namely, following (Del Popolo et al. 2020b), the NSs mass is already on the plateau region. However, if we take a close look on how the NS mass changes close to the clump outskirt, we start to see some structure in the NS mass distribution.

The obtained results are based on the techniques described. The

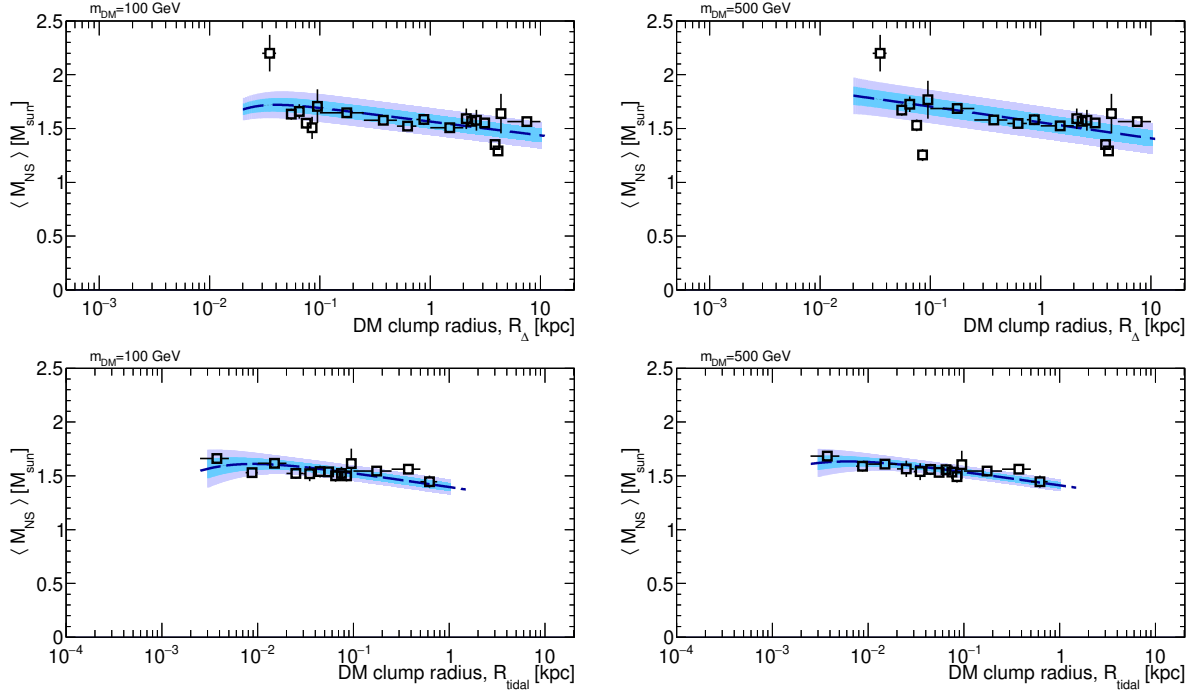


Figure 10. Fits to the NSs mass as a function of the clump radius (top) and tidal clump radius (bottom). Clumps were selected in the vicinity of 0.01, 0.05, 0.1, 0.25, 0.5, 0.75, 1, 2, and 5 kpc to the NSs, clumps scale was requested to be greater than this separation distance. Left: using the DM mass $m_{\text{dm}} = 100 \text{ GeV}$. Right: using the DM mass $m_{\text{dm}} = 500 \text{ GeV}$.

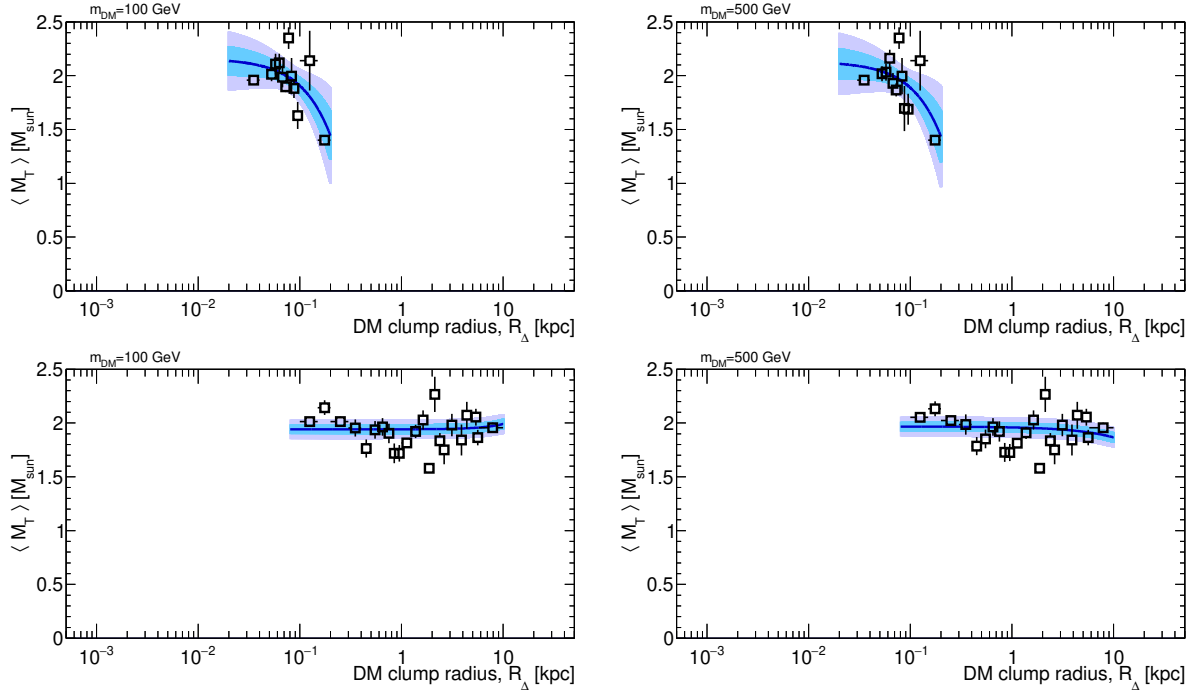


Figure 11. Fits to the total mass of the binary systems as a function of the clump radius. Top: Clumps were selected in the vicinity of 0.05 kpc to the NSs, clumps scale was requested to be greater than this separation distance ($> 0.05 \text{ kpc}$). Bottom: Clumps were selected in the vicinity of 0.1 kpc to the NSs, clumps scale was requested to be greater than this separation distance ($> 0.1 \text{ kpc}$). Left: using the DM mass $m_{\text{dm}} = 100 \text{ GeV}$. Right: using the DM mass $m_{\text{dm}} = 500 \text{ GeV}$. Fits performed with the help of the power law function.

clumpy morphology of galaxies has been produced by the idealized cosmological numerical simulations of isolated galaxies with the help of CLUMPY. Using simulations with feedback models as realistic as possible and in a full cosmological context is the most promising way to improve our understanding of the nature of star-forming clumps and the relations between clumps and NSs.

The reliability of the EoS constraints depends on the degree to which systematic errors can be controlled (in many current analyses, these errors are significantly larger than the formal statistical uncertainties; see [Miller 2020](#); [Miller & Lamb 2016](#)), as well as on the precision of the astrophysical models that are applied to the data.

Because neither model atmosphere spectra (e.g., [Suleimanov et al. 2012](#)) nor the most accurately measured observed spectra ([Miller et al. 2011](#)) are exactly Planckian, using Planck fits as proxies throws away information and could even introduce biases.

All current methods for determining the radii of NSs using their X-ray fluxes and spectra are subject to astrophysical effects that can confuse or bias the radius measurement. Furthermore, in most cases the data are not yet precise enough to determine whether the model being used correctly describes the data. It is therefore possible that a model may provide a statistically good fit and an apparently tight radius constraint but a value for the radius that is strongly biased relative to the true value.

There are recent developments on this subject ([Nättilä et al. 2017](#)) which aimed to assess the accuracy of future measurement methods and to explore possible biases in the results. Due to these experimental challenges, the radius measurements for the observed NSs are reported less frequently than their mass measurements, see Tables [A1-A2](#).

Therefore, our analysis has benefited from recent advancements in technology, which provide unprecedented mass and distance measurements of the known NSs. Significant effort has been spent attempting to simulate the DM clumps distribution in the Galaxy, as well as to link this distribution to other aspects of DM clumps phenomenology.

The results from this research will provide valuable knowledge of the Galactic pulsar population for the planning of future DM survey strategies.

However, our efforts are intrinsically constrained by those pulsars which are currently known and available for study. The properties of the NSs that were used, are collected in Tables [A1-A2](#). Further characterizing the population statistics of NSs will allow for a greater understanding of the pulsar population and DM distribution as a whole and will be vital in the planning of future pulsars and DM surveys to be undertaken with next-generation radio telescopes such as MeerKAT ([Bailes et al. 2020](#)), the Square Kilometre Array (SKA) ([Dutta et al. 2022](#)) and the Five-hundred-meter Aperture Spherical Telescope (FAST) ([Hu et al. 2020](#)). A more mature judgment can be formed when the number of the measured NS masses will increase by a factor of 5-10 from those discovered thus far. Apart from that, a major caveat in the estimation of DM clump mapping/detection is that our understanding of the underlying NSs distribution is still inadequate and hampered by the small number of known NSs, and the measured uncertainties of the NS masses.

NSs formed in the DMCs could be detectable by next-generation GW detectors, such as Advanced LIGO ([Aasi et al. 2015](#)), Advanced Virgo ([Acernese et al. 2015](#)), KAGRA ([Somiya 2012](#)), and the proposed space-based detector LISA ([Amaro-Seoane et al. 2017](#)). If the NS merger is accompanied by an electromagnetic counterpart, the GW source can be localized and a redshift can be determined. Knowing the redshift of the source allows us to infer its luminosity distance, which in turn constrains the distance between the source and

the Earth. The distance to the source can then be used to infer NS properties, such as its mass, spin, and EoS. The NS distances inferred through dispersion measures exhibit appreciable variety and are susceptible to biases ([Verbiest et al. 2012](#)), a typical measurement uncertainty of $\sim 20\%$ is not unreasonable ([Taylor & Cordes 1993](#); [Yao et al. 2017](#)), and indeed is expected to be readily achievable with next-generation radio telescopes ([Smits et al. 2011](#)).

The most promising GW sources from DMCs are expected to be low-mass binary NSs (LMBNSs). Low-mass binary systems are expected to form in DMCs due to the high stellar densities, which can lead to dynamical exchanges and three-body interactions ([Berezinsky et al. 2014](#)).

If the merging NSs have masses of $\sim 1.2M_{\odot}$, the corresponding GW signal might be detectable.

Another option is to detect dark clumps via gravitational perturbations of visible objects ([Penarrubia et al. 2010](#)). In this regard very wide binaries, i.e. those with separations $a \gtrsim 100$ AU, may enable simple experiments to test for the presence of dark substructures (clumps, halos), for even extremely weak tidal perturbations can disrupt them. In the stellar halo of the Milky Way, perturbers can be identified as inhomogeneities in the Galactic potential. There are huge list of different perturbers on such binaries, therefore isolation of such an effect is not straightforward. See the recent report on this subject in [Inoue et al. \(2023\)](#).

Ref. ([Penarrubia et al. 2010](#)) studied the disruption of wide ($\gtrsim 100$ AU) binaries as a result of interactions with dark substructures orbiting in dwarf galaxies, as well as exploring whether the effects can be detected with our present observational capabilities.

If there exists in nature dark matter clumps with compactness $GM/(Rc^2) \gtrsim 0.1$, i.e. comparable with neutron stars, GWs emitted during tidal encounters could be measured by ground-based detectors, such as LIGO ([Mendes & Yang 2017](#)).

ACKNOWLEDGEMENTS

We wish to acknowledge the support of the UniGe HPC center, which helps us to simulate galaxies. ADP thanks the Institute of Astronomy of the Academy of Science in Sofia for the hospitality. MLeD acknowledges the financial support by the Lanzhou University starting fund, the Fundamental Research Funds for the Central Universities (Grant No. lzujbky-2019-25), National Science Foundation of China (grant No. 12047501) and the 111 Project under Grant No. B20063.

DATA AVAILABILITY

The CLUMPY synthetic data underlying this paper are publicly available. In case of the data loss, it can be reproduced with the help of the configuration parameters provided by authors. The code that supports the findings of this study will be shared upon a reasonable request to the corresponding author.

REFERENCES

- Aad G., et al., 2023, *JHEP*, 07, 116
- Aalseth C. E., et al., 2011, *Phys. Rev. Lett.*, 106, 131301
- Aasi J., et al., 2015, *Class. Quant. Grav.*, 32, 074001
- Abbott, T. M. C. and others 2023, *Phys. Rev. D*, 107, 023531
- Abbott T. M. C., et al., 2022, *Phys. Rev. D*, 105, 023520
- Abdalla E., Abramo L. R. W., Sodre Jr. L., Wang B., 2009, *Phys. Lett.*, B673, 107

- Abdalla E., Abramo L. R., de Souza J. C. C., 2010, *Phys. Rev.*, D82, 023508
- Acernese F., et al., 2015, *Class. Quant. Grav.*, 32, 024001
- Ackermann M., et al., 2015, *Phys. Rev. Lett.*, 115, 231301
- Ade P. A. R., et al., 2014, *Astron. Astrophys.*, 571, A16
- Agnese R., et al., 2014, *Phys. Rev. Lett.*, 112, 041302
- Akerib D. S., et al., 2017, *Phys. Rev. Lett.*, 118, 021303
- Ali-Haïmoud Y., Kovetz E. D., Silk J., 2016, *Phys. Rev. D*, 93, 043508
- Alonso-Álvarez G., Jaeckel J., 2018, *JCAP*, 10, 022
- Alsing J., Silva H. O., Berti E., 2018, *Mon. Not. Roy. Astron. Soc.*, 478, 1377
- Amaro-Seoane P., et al., 2017, arXiv:1702.00786[astro-ph.IM]
- Andersen B. C., Ransom S. M., 2018, *Astrophys. J. Lett.*, 863, L13
- Antoniadis J., van Kerkwijk M. H., Koester D., Freire P. C. C., Wex N., Tauris T. M., Kramer M., Bassa C. G., 2012, *Mon. Not. Roy. Astron. Soc.*, 423, 3316
- Antoniadis J., et al., 2013, *Science*, 340, 6131
- Aprile E., et al., 2012, *Phys. Rev. Lett.*, 109, 181301
- Aprile E., et al., 2016, *Phys. Rev. D*, 94, 122001
- Aprile E., et al., 2022, *Phys. Rev. Lett.*, 129, 161805
- Archibald A. M., et al., 2018, *Nature*, 559, 73
- Armand C., Herrmann B., 2022, *JCAP*, 11, 055
- Arzoumanian Z., et al., 2018, *Astrophys. J. Suppl.*, 235, 37
- Aslanyan G., Price L. C., Adams J., Bringmann T., Clark H. A., Easter R., Lewis G. F., Scott P., 2016, *Phys. Rev. Lett.*, 117, 141102
- Bailes M., et al., 2020, *Publ. Astron. Soc. Austral.*, 37, e028
- Bak Nielsen A.-S., Patruno A., D'Angelo C., 2017, *Mon. Not. Roy. Astron. Soc.*, 468, 824
- Balakrishnan V., et al., 2023, *Astrophys. J. Lett.*, 942, L35
- Barr E. D., Freire P. C. C., Kramer M., Champion D. J., Berezhina M., Bassa C. G., Lyne A. G., Stappers B. W., 2017, *Mon. Not. Roy. Astron. Soc.*, 465, 1711
- Bassa C. G., van Kerkwijk M. H., Koester D., Verbunt F., 2006, *Astron. Astrophys.*, 456, 295
- Bell J. F., Bessell M. S., Stappers B. W., Bailes M., Kaspi V. M., 1995, *Astrophys. J. Lett.*, 447, L117
- Bell N. F., Busoni G., Robles S., Virgato M., 2020, *JCAP*, 09, 028
- Bellm E. C., et al., 2016, *Astrophys. J.*, 816, 74
- Berezina M., et al., 2017, *Mon. Not. Roy. Astron. Soc.*, 470, 4421
- Berezinsky V., Dokuchaev V., Eroshenko Y., 2003, *Phys. Rev. D*, 68, 103003
- Berezinsky V. S., Dokuchaev V. I., Eroshenko Y. N., 2005, *The Identification of Dark Matter*, pp 81–86
- Berezinsky V., Dokuchaev V., Eroshenko Y., 2006, *Phys. Rev. D*, 73, 063504
- Berezinsky V. S., Dokuchaev V. I., Eroshenko Y. N., 2013, *JCAP*, 11, 059
- Berezinsky V. S., Dokuchaev V. I., Eroshenko Y. N., 2014, *Phys. Usp.*, 57, 1
- Bernabei R., et al., 2010, *Eur. Phys. J. C*, 67, 39
- Berthereau A., et al., 2023, *Astron. Astrophys.*, 674, A71
- Bertolami O., Gil Pedro F., Le Delliou M., 2007, *Phys. Lett.*, B654, 165
- Bertolami O., Gil Pedro F., Le Delliou M., 2008, *EAS Publ. Ser.*, 30, 161
- Bertolami O., Pedro F. G., Le Delliou M., 2009, *Gen. Rel. Grav.*, 41, 2839
- Bertolami O., Gil Pedro F., Le Delliou M., 2012, *Gen. Rel. Grav.*, 44, 1073
- Bertone G., Fairbairn M., 2008, *Phys. Rev.*, D77, 043515
- Bertschinger E., 1985, *Astrophys. J. Suppl.*, 58, 39
- Betoule M., et al., 2014, *Astron. Astrophys.*, 568, A22
- Bhalerao V., van Kerkwijk M. H., Harrison F., 2012a, *Astrophys. J.*, 757, 10
- Bhalerao V. B., van Kerkwijk M. H., Harrison F. A., 2012b, *The Astrophysical Journal*, 757, 10
- Bhat S. A., Paul A., 2020, *Eur. Phys. J. C*, 80, 544
- Bhat N. D. R., Bailes M., Verbiest J. P. W., 2008, *Phys. Rev. D*, 77, 124017
- Bonaca A., Hogg D. W., Price-Whelan A. M., Conroy C., 2018, J. 10.3847/1538-4357/ab2873
- Bonnivard V., et al., 2015, *Mon. Not. Roy. Astron. Soc.*, 453, 849
- Bonnivard V., Hütten M., Nezri E., Charbonnier A., Combet C., Maurin D., 2016a, *Comput. Phys. Commun.*, 200, 336
- Bonnivard V., Maurin D., Walker M. G., 2016b, *Mon. Not. Roy. Astron. Soc.*, 462, 223
- Bringmann T., 2009, *New J. Phys.*, 11, 105027
- Bringmann T., Scott P., Akrami Y., 2012, *Phys. Rev. D*, 85, 125027
- Bullock J. S., Kolatt T. S., Sigad Y., Somerville R. S., Kravtsov A. V., Klypin A. A., Primack J. R., Dekel A., 2001, *Mon. Not. Roy. Astron. Soc.*, 321, 559
- Cameron A. D., et al., 2018, *Mon. Not. Roy. Astron. Soc.*, 475, L57
- Cameron A. D., et al., 2020, *Mon. Not. Roy. Astron. Soc.*, 493, 1063
- Cameron A. D., et al., 2022, in 16th Marcel Grossmann Meeting on Recent Developments in Theoretical and Experimental General Relativity, Astrophysics and Relativistic Field Theories. (arXiv:2203.15995), doi:10.1142/9789811269776_0312
- Casares J., Hernandez J. I. G., Israeli G., Rebolo R., 2010, *Mon. Not. Roy. Astron. Soc.*, 401, 2517
- Charbonnier A., et al., 2011, *Mon. Not. Roy. Astron. Soc.*, 418, 1526
- Charbonnier A., Combet C., Maurin D., 2012, *Comput. Phys. Commun.*, 183, 656
- Chatrchyan S., et al., 2012, *JHEP*, 09, 094
- Chen W., et al., 2023, *Mon. Not. Roy. Astron. Soc.*, 520, 3847
- Ciarcelluti P., Sandin F., 2011, *Phys. Lett.*, B695, 19
- Cirelli M., et al., 2011, *JCAP*, 03, 051
- Clark C. J., et al., 2021, *Mon. Not. Roy. Astron. Soc.*, 502, 915
- Cocozza G., Ferraro F. R., Possenti A., D'Amico N., 2006, *Astrophys. J. Lett.*, 641, L129
- Combet C., Maurin D., Nezri E., Pointecouteau E., Hinton J. A., White R., 2012, *Phys. Rev. D*, 85, 063517
- Conrad J., 2014, in Interplay between Particle and Astroparticle physics (IPA2014) London, United Kingdom, August 18-22, 2014. (arXiv:1411.1925), <http://inspirehep.net/record/1326617/files/arXiv:1411.1925.pdf>
- Corongiu A., et al., 2012, *Astrophys. J.*, 760, 100
- Dai D.-C., Stojkovic D., 2009, *JHEP*, 08, 052
- Das A., Malik T., Nayak A. C., 2019, *Phys. Rev. D*, 99, 043016
- Das H. C., Kumar A., Kumar B., Kumar Biswal S., Nakatsukasa T., Li A., Patra S. K., 2020, *Mon. Not. Roy. Astron. Soc.*, 495, 4893
- Das A., Malik T., Nayak A. C., 2022, *Phys. Rev. D*, 105, 123034
- Del Popolo A., Le Delliou M., Deliyergiyev M., 2020a, *Universe*, 6, 222
- Del Popolo A., Deliyergiyev M., Le Delliou M., Tolos L., Burgio F., 2020b, *Phys. Dark Univ.*, 28, 100484
- Del Popolo A., Deliyergiyev M., Le Delliou M., 2020c, *Phys. Dark Univ.*, 30, 100622
- Del Popolo A., Deliyergiyev M., Le Delliou M., Tolos L., Burgio F., 2020d, PoS, EPS-HEP2019, 098
- Deliyergiyev M., Del Popolo A., Tolos L., Le Delliou M., Lee X., Burgio F., 2019, *Phys. Rev. D*, 99, 063015
- Demorest P., Pennucci T., Ransom S., Roberts M., Hessels J., 2010, *Nature*, 467, 1081
- Desvignes G., et al., 2016, *Mon. Not. Roy. Astron. Soc.*, 458, 3341
- Diemand J., Kuhlen M., Madau P., Zemp M., Moore B., Potter D., Stadel J., 2008, *Nature*, 454, 735
- Dutta K., Ghosh A., Kar A., Mukhopadhyaya B., 2022, *JCAP*, 09, 005
- Eke V. R., Navarro J. F., Steinmetz M., 2001, *Astrophys. J.*, 554, 114
- Ellis J., Hütsi G., Kannike K., Marzola L., Raidal M., Vaskonen V., 2018, *Phys. Rev.*, D97, 123007
- Falanga M., Bozzo E., Lutovinov A., Bonnet-Bidaud J. M., Fetisova Y., Puls J., 2015, *Astron. Astrophys.*, 577, A130
- Fan Y.-z., Yang R.-z., Chang J., 2012, preprint, (arXiv:1204.2564)
- Ferdman R. D., 2017, *IAU Symp.*, 337, 146
- Ferdman R. D., et al., 2014, *Mon. Not. Roy. Astron. Soc.*, 443, 2183
- Ferdman R. D., et al., 2020, *Nature*, 583, 211
- Fonseca E., Stairs I. H., Thorsett S. E., 2014, *Astrophys. J.*, 787, 82
- Fonseca E., et al., 2016, *Astrophys. J.*, 832, 167
- Fornasa M., et al., 2013, *Mon. Not. Roy. Astron. Soc.*, 429, 1529
- Fortin M., Bejger M., Haensel P., Zdunik J. L., 2016, *Astron. Astrophys.*, 586, A109
- Freire P. C. C., 2008, *AIP Conf. Proc.*, 983, 459
- Freire P. C. C., Ransom S. M., Begin S., Stairs I. H., Hessels J. W. T., Frey L. H., Camilo F., 2008a, *Astrophys. J.*, 675, 670
- Freire P. C. C., Wolszczan A., Berg M. v. d., Hessels J. W. T., 2008b, *Astrophys. J.*, 679, 1433
- Gao L., White S. D. M., Jenkins A., Stoehr F., Springel V., 2004, *Mon. Not. Roy. Astron. Soc.*, 355, 819

- Gelino D. M., Tomsick J. A., Heindl W. A., 2002, Bulletin of the American Astronomical Society, **201**, 54.05
- Goldman I., Nussinov S., 1989, *Phys. Rev.*, D40, 3221
- Goldman I., Mohapatra R. N., Nussinov S., Rosenbaum D., Teplitz V., 2013, *Phys. Lett.*, B725, 200
- Gonzalez-Caniulef D., Guillot S., Reisenegger A., 2019, *Mon. Not. Roy. Astron. Soc.*, 490, 5848
- Green A. M., 2017, *J. Phys. G*, 44, 084001
- Guillot S., et al., 2019, *Astrophys. J. Lett.*, 887, L27
- Guo Y. J., et al., 2021, *Astron. Astrophys.*, 654, A16
- Guver T., Ozel F., Cabrera-Lavers A., Wroblewski P., 2010a, *Astrophys. J.*, 712, 964
- Guver T., Wroblewski P., Camarota L., Ozel F., 2010b, *Astrophys. J.*, 719, 1807
- Güver T., Emre Erkoca A., Hall Reno M., Sarcevic I., 2014, *J. Cosmology Astropart. Phys.*, 5, 013
- Haniewicz H. T., Ferdman R. D., Freire P. C. C., Champion D. J., Bunting K. A., Lorimer D. R., McLaughlin M. A., 2020, *Mon. Not. Roy. Astron. Soc.*, 500, 4620
- Hildebrandt H., et al., 2017, *Mon. Not. Roy. Astron. Soc.*, 465, 1454
- Hobbs G., et al., 2004, *Mon. Not. Roy. Astron. Soc.*, 352, 1439
- Hu W., Wang X., Wu F., Wang Y., Zhang P., Chen X., 2020, *Mon. Not. Roy. Astron. Soc.*, 493, 5854
- Inoue K. T., Minezaki T., Matsushita S., Nakanishi K., 2023, *Astrophys. J.*, 954, 197
- Jacoby B. A., Cameron P. B., Jenet F. A., Anderson S. B., Murty R. N., Kulkarni S. R., 2006, *Astrophys. J. Lett.*, 644, L113
- Jennings R. J., Kaplan D. L., Chatterjee S., Cordes J. M., Deller A. T., 2018, *Astrophys. J.*, 864, 26
- Jiang L., Wang N., Chen W.-C., Liu W.-M., Leng C.-w., Yuan J.-P., Qian X.-L., 2021, *Res. Astron. Astrophys.*, 21, 231
- Kandel D., Romani R. W., 2020, *The Astrophysical Journal*, 892, 101
- Kandel D., Romani R. W., 2023, *Astrophys. J.*, 942, 6
- Kaplan D. L., Bhalerao V. B., van Kerkwijk M. H., Koester D., Kulkarni S. R., Stovall K., 2013, *Astrophys. J.*, 765, 158
- Karkevandi D. R., Shakeri S., Sagun V., Ivanytskyi O., 2022, *Phys. Rev. D*, 105, 023001
- Keith M. J., Kramer M., Lyne A. G., Eatough R. P., Stairs I. H., Possenti A., Camilo F., Manchester R. N., 2009, *Mon. Not. Roy. Astron. Soc.*, 393, 623
- Kennedy M. R., et al., 2022, *Mon. Not. Roy. Astron. Soc.*, 512, 3001
- Kiziltan B., Kottas A., De Yoreo M., Thorsett S. E., 2013, *Astrophys. J.*, 778, 66
- Kolb E. W., Tkachev I. I., 1994, *Phys. Rev. D*, 50, 769
- Komatsu E., 2003, in 4th International Conference on Physics Beyond the Standard Model: Beyond the Desert (BEYOND 03). pp 75–91
- Komatsu E., et al., 2009, *Astrophys. J. Suppl.*, 180, 330
- Konacki M., Wolszczan A., 2003, *Astrophys. J. Lett.*, 591, L147
- Kouvaris C., 2008, *Phys. Rev. D*, 77, 023006
- Kouvaris C., 2013, preprint, ([arXiv:1308.3222](https://arxiv.org/abs/1308.3222))
- Kouvaris C., Nielsen N. G., 2015, *Phys. Rev.*, D92, 063526
- Kouvaris C., Tinyakov P., 2010, *Phys. Rev.*, D82, 063531
- Kouvaris C., Tinyakov P., 2011a, *Phys. Rev. D*, 83, 083512
- Kouvaris C., Tinyakov P., 2011b, *Phys. Rev. Lett.*, 107, 091301
- Kouvaris C., Langæble K., Nielsen N. G., 2016, *JCAP*, 10, 012
- Kramer M., et al., 2021, *Phys. Rev. X*, 11, 041050
- Lattimer J. M., Prakash M., 2004, *Science*, 304, 536
- Law D. R., Majewski S. R., Johnston K. V., 2009, *Astrophys. J. Lett.*, 703, L67
- Le Dellou M., Bertolami O., Gil Pedro F., 2007, *AIP Conf. Proc.*, 957, 421
- Le Dellou M., Marcondes R. J. F., Lima Neto G. B., Abdalla E., 2015, *Mon. Not. Roy. Astron. Soc.*, 453, 2
- Le Dellou M., Marcondes R. J. F., Neto G. a. B. L., 2019, *Mon. Not. Roy. Astron. Soc.*, 490, 1944
- Leung S. C., Chu M. C., Lin L. M., 2011, *Phys. Rev.*, D84, 107301
- Li A., Huang F., Xu R.-X., 2012, *Astropart. Phys.*, 37, 70
- Linares M., Shahbaz T., Casares J., 2018, *Astrophys. J.*, 859, 54
- Liu K., et al., 2020, *Mon. Not. Roy. Astron. Soc.*, 499, 2276
- Lohmer O., Kramer M., Driebe T., Jessner A., Mitra D., Lyne A. G., 2004, *Astron. Astrophys.*, 426, 631
- Lynch R. S., Freire P. C. C., Ransom S. M., Jacoby B. A., 2012, *Astrophys. J.*, 745, 109
- Lynch R. S., et al., 2018, *Astrophys. J.*, 859, 93
- Madau P., Diemand J., Kuhlen M., 2008, *Astrophys. J.*, 679, 1260
- Mason A. B., Norton A. J., Clark J. S., Negueruela I., Roche P., 2010, *Astron. Astrophys.*, 509, A79
- Mason A. B., Clark J. S., Norton A. J., Crowther P. A., Tauris T. M., Langer N., Negueruela I., Roche P., 2012, *Mon. Not. Roy. Astron. Soc.*, 422, 199
- Mata Sánchez D., Istrate A. G., van Kerkwijk M. H., Breton R. P., Kaplan D. L., 2020, *Mon. Not. Roy. Astron. Soc.*, 494, 4031
- Maurin D., Combet C., Nezri E., Pointecouteau E., 2012, *Astron. Astrophys.*, 547, A16
- McCullough M., Fairbairn M., 2010, *Phys. Rev.*, D81, 083520
- McDermott S. D., Yu H.-B., Zurek K. M., 2012, *Phys. Rev. D*, 85, 023519
- McKee J. W., et al., 2020, *Mon. Not. Roy. Astron. Soc.*, 499, 4082
- Mendes R. F. P., Yang H., 2017, *Class. Quant. Grav.*, 34, 185001
- Mignani R. P., Corongiu A., Pallanca C., Ferraro F. R., 2013, *Mon. Not. Roy. Astron. Soc.*, 430, 1008
- Miller M. C., 2020, *Astrophys. Space Sci. Libr.*, 461, 1
- Miller M. C., Lamb F. K., 2016, *Eur. Phys. J. A*, 52, 63
- Miller M. C., Boutloukos S., Lo K. H., Lamb F. K., 2011
- Miller M. C., et al., 2021, *Astrophys. J. Lett.*, 918, L28
- Moldon J., Ribo M., Paredes J. M., Brisken W., Dhawan V., Kramer M., Lyne A. G., Stappers B. W., 2012, *Astron. Astrophys.*, 543, A26
- Moliné A., Sánchez-Conde M. A., Palomares-Ruiz S., Prada F., 2017, *Mon. Not. Roy. Astron. Soc.*, 466, 4974
- Mukhopadhyay P., Schaffner-Bielich J., 2016, *Phys. Rev.*, D93, 083009
- Näyttälä J., Miller M. C., Steiner A. W., Kajava J. J. E., Suleimanov V. F., Poutanen J., 2017, *Astron. Astrophys.*, 608, A31
- Nesti F., Salucci P., 2013, *JCAP*, 07, 016
- Nezri E., White R., Combet C., Maurin D., Pointecouteau E., Hinton J. A., 2012, *Mon. Not. Roy. Astron. Soc.*, 425, 477
- Ng C., et al., 2015, *Mon. Not. Roy. Astron. Soc.*, 450, 2922
- Ng C., Guillemot L., Freire P. C. C., Kramer M., Champion D. J., Cognard I., Theureau G., Barr E. D., 2020, *Mon. Not. Roy. Astron. Soc.*, 493, 1261
- Nice D. J., Splaver E. M., Stairs I. H., 2001, *Astrophys. J.*, 549, 516
- Oppenheimer J. R., Volkoff G. M., 1939, *Phys. Rev.*, 55, 374
- Orosz J. A., van Kerkwijk M. H., 2003, *Astron. Astrophys.*, 397, 237
- Panopopoulos G., Lopes I., 2017, *Phys. Rev. D*, 96, 083004
- Penarrubia J., Koposov S. E., Walker M. G., Gilmore G., Evans N. W., Mackay C. D., 2010, arXiv:1005.5388[astro-ph.GA]
- Perez-Garcia M. A., Silk J., 2012, *Phys. Lett.*, B711, 6
- Perez-Garcia M. A., Silk J., Stone J. R., 2010, *Phys. Rev. Lett.*, 105, 141101
- Pérez de los Heros C., 2020, *Symmetry*, 12, 1648
- Pieri L., Bertone G., Branchini E., 2008, *Mon. Not. Roy. Astron. Soc.*, 384, 1627
- Posselet B., Schreyer K., Perna R., Sommer M. W., Klein B., Slane P., 2010, *Mon. Not. Roy. Astron. Soc.*, 405, 1840
- Ransom S. M., et al., 2014, *Nature*, 505, 520
- Rawls M. L., Orosz J. A., McClintock J. E., Torres M. A. P., Bailyn C. D., Buxton M. M., 2011, *Astrophys. J.*, 730, 25
- Reardon D. J., et al., 2016, *Mon. Not. Roy. Astron. Soc.*, 455, 1751
- Reardon D. J., et al., 2021, *Mon. Not. Roy. Astron. Soc.*, 507, 2137
- Rezzolla L., Most E. R., Weih L. R., 2018, *Astrophys. J.*, 852, L25
- Ricotti M., Gould A., 2009, *ApJ*, 707, 979
- Ridolfi A., Freire P. C. C., Gupta Y., Ransom S. M., 2019, *Mon. Not. Roy. Astron. Soc.*, 490, 3860
- Ridolfi A., et al., 2021, *Mon. Not. Roy. Astron. Soc.*, 504, 1407
- Riley T. E., et al., 2019, *Astrophys. J. Lett.*, 887, L21
- Riley T. E., et al., 2021, *Astrophys. J. Lett.*, 918, L27
- Romani R. W., Kandel D., Filippenko A. V., Brink T. G., Zheng W., 2021, *Astrophys. J. Lett.*, 908, L46
- Romani R. W., Kandel D., Filippenko A. V., Brink T. G., Zheng W., 2022, *Astrophys. J. Lett.*, 934, L18
- Roy J., et al., 2015, *Astrophys. J. Lett.*, 800, L12
- Sandin F., Ciarcelluti P., 2009, *Astropart. Phys.*, 32, 278

- Schaffner-Bielich J., 2005, *Journal of Physics G: Nuclear and Particle Physics*, 31, S651
- Schmid C., Schwarz D. J., Widerin P., 1999, *Phys. Rev. D*, 59, 043517
- Schnitzeler D. H. F. M., Eatough R. P., Ferrière K., Kramer M., Lee K. J., Noutsos A., Shannon R. M., 2016, *Mon. Not. Roy. Astron. Soc.*, 459, 3005
- Scott P., Sivertsson S., 2009, *Phys. Rev. Lett.*, 103, 211301
- Sedrakian A., 2019, *Phys. Rev. D*, 99, 043011
- Serylak M., et al., 2022, *Astron. Astrophys.*, 665, A53
- Shahbaz T., Linares M., Rodriguez-Gil P., Casares J., 2019, *Mon. Not. Roy. Astron. Soc.*, 488, 198
- Shao D.-S., Tang S.-P., Jiang J.-L., Fan Y.-Z., 2020, *Phys. Rev. D*, 102, 063006
- Shaw A. W., Heinke C. O., Steiner A. W., Campana S., Cohn H. N., Ho W. C. G., Lugger P. M., Servillat M., 2018, *Mon. Not. Roy. Astron. Soc.*, 476, 4713
- Silk J., Stebbins A., 1993, *Astrophys. J.*, 411, 439
- Sirunyan A., et al., 2021, *JHEP*, 03, 011
- Smits R., Tingay S. J., Wex N., Kramer M., Stappers B., 2011, *Astron. Astrophys.*, 528, A108
- Somiya K., 2012, *Class. Quant. Grav.*, 29, 124007
- Springel V., et al., 2008, *Mon. Not. Roy. Astron. Soc.*, 391, 1685
- Stairs I. H., Thorsett S. E., Taylor J. H., Wolszczan A., 2002, *Astrophys. J.*, 581, 501
- Stovall K., et al., 2019, *Astrophys. J.*, 870, 74
- Strader J., Li K.-L., Chomiuk L., Heinke C. O., Udalski A., Peacock M., Shishkovsky L., Tremou E., 2016, *Astrophys. J.*, 831, 89
- Strader J., et al., 2019, *Astrophys. J.*, 872, 42
- Suleimanov V., Poutanen J., Werner K., 2012, *Astron. Astrophys.*, 545, A120
- Swiggum J. K., et al., 2015, *Astrophys. J.*, 805, 156
- Swihart S. J., et al., 2017, *Astrophys. J.*, 851, 31
- Tan A., et al., 2016, *Phys. Rev. Lett.*, 117, 121303
- Tauris T. M., Janka H.-T., 2019, *Astrophys. J. Lett.*, 886, L20
- Taylor J. H., Cordes J. M., 1993, *Astrophys. J.*, 411, 674
- Thorsett S. E., Chakrabarty D., 1999, *Astrophys. J.*, 512, 288
- Thorsett S. E., Arzoumanian Z., Taylor J. H., 1993, *ApJ*, 412, L33
- Tolman R. C., 1939, *Phys. Rev.*, 55, 364
- Tolos L., Schaffner-Bielich J., Dengler Y., 2015, *Phys. Rev. D*, 92, 123002
- Trigo M. D., Boirin L., Costantini E., Mendez M., Parmar A., 2011, *Astron. Astrophys.*, 528, A150
- Trumper J. E., Burwitz V., Haberl F., Zavlin V. E., 2004, *Nucl. Phys. B Proc. Suppl.*, 132, 560
- Tumasyan A., et al., 2022, *JHEP*, 06, 156
- Ullio P., Bergstrom L., Edsjo J., Lacey C. G., 2002, *Phys. Rev. D*, 66, 123502
- Val Baker, A. K. F. Norton, A. J. Quaintrell, H. 2005, *A&A*, 441, 685
- Venkatraman Krishnan V., et al., 2020, *Science*, 367, 577
- Verbiest J. P. W., et al., 2008, *Astrophys. J.*, 679, 675
- Verbiest J. P. W., Weisberg J. M., Chael A. A., Lee K. J., Lorimer D. R., 2012, *Astrophys. J.*, 755, 39
- Walker M. G., Combet C., Hinton J. A., Maurin D., Wilkinson M. I., 2011, *Astrophys. J. Lett.*, 733, L46
- Walker M. G., et al., 2016, *Astrophys. J.*, 819, 53
- Wang J., Bose S., Frenk C. S., Gao L., Jenkins A., Springel V., White S. D. M., 2020a, *Nature*, 585, 39
- Wang L., et al., 2020b, *The Astrophysical Journal*, 892, 43
- Wechsler R. H., Bullock J. S., Primack J. R., Kravtsov A. V., Dekel A., 2002, *Astrophys. J.*, 568, 52
- Weisberg J. M., Huang Y., 2016, *Astrophys. J.*, 829, 55
- Xiang Q.-F., Jiang W.-Z., Zhang D.-R., Yang R.-Y., 2014, *Phys. Rev.*, C89, 025803
- Yang R.-J., Gao X.-T., 2011, *Classical and Quantum Gravity*, 28, 065012
- Yang Y.-Y., Zhang C.-M., Li D., Wang D.-H., Pan Y.-Y., Lingfu R.-F., Zhou Z.-W., 2017, *The Astrophysical Journal*, 835, 185
- Yao J. M., Manchester R. N., Wang N., 2017, *The Astrophysical Journal*, 835, 29
- Zhang C. M., et al., 2011, *Astron. Astrophys.*, 527, A83
- Zhang Z. Y., et al., 2022, *Phys. Rev. Lett.*, 129, 221301
- Zheng H., Chen L.-W., 2016, *ApJ*, 831, 127
- Zheng R., Huang Q.-G., 2011, *J. Cosmology Astropart. Phys.*, 3, 2
- Zhu W. W., et al., 2019, *Astrophys. J.*, 881, 165
- de Lavallaz A., Fairbairn M., 2010, *Phys. Rev.*, D81, 123521
- van Leeuwen J., et al., 2015, *Astrophys. J.*, 798, 118
- Özel F., Gould A., Güver T., 2012, *The Astrophysical Journal*, 748, 5

APPENDIX A: NEUTRON STARS TABLES

Table A1. List of the examined neutron stars, where (a) NS-NS binary system, (b) NS in X-ray binaries, (c) radio MSP, (d1) WD-NS system, (d2) WD-NS GalCluster pulsar. The gray entities are shown for the cross-check, taken from the references used in (Shao et al. 2020).

| Name | Gal. latitude, b , [deg] | Gal. longitude, l , [deg] | distance, [kpc] | NS mass, [M_{\odot}] | Comp. star mass, [M_{\odot}] | NS radius, [km] | Age τ_c [Gyr] |
|--|-------------------------------|--------------------------------|--|--|--|---|---|
| (b) 4U 1820-30(Guver et al. 2010b) | -7.9138 | 2.7882 | 8.4 | 1.58 ^{+0.06} _{-0.05} | — | 9.11 ^{+0.4} _{-0.4} | — |
| (a) B1534+12 (Stairs et al. 2002; Kiziltan et al. 2013) | 48.34 | 19.85 | 1.051 | 1.333 ^{+0.001} _{-0.001} | 1.342 ^{+0.001} _{-0.001} | — | 0.248 (Mignani et al. 2013) |
| (a) B1534+12 (Fonseca et al. 2014) | 48.34143147 | 19.8475262 | 1.051 ^{+0.005} _{-0.005} | 1.333 ^{+0.002} _{-0.002} | 1.345 ^{+0.002} _{-0.002} | — | — |
| (a) B1913+16 (Weisberg & Hume 2016; Kiziltan et al. 2013) | 2.122 | 49.968 | 4.167 | 1.439 ^{+0.002} _{-0.002} | 1.388 ^{+0.002} _{-0.002} | — | 0.108 (Mignani et al. 2013) |
| (a) B2127+11C (Jacoby et al. 2006; Kiziltan et al. 2013) | -27.32 | 65.03 | 10.4 | 1.356 ^{+0.001} _{-0.001} | 1.354 ^{+0.001} _{-0.001} | — | 0.097 (Mignani et al. 2013) |
| (a) B2303+46 (Zhang et al. 2011) | -12.021 | 104.931 | 3.159 | 1.38 ^{+0.01} _{-0.01} | 1.37 ^{+0.01} _{-0.01} | — | 0.0297 (Mignani et al. 2013) |
| (a) B2303+46 (Thorsett & Chakrabarty 1999) | -12.021 | 104.931 | 3.159 | 1.34 ^{+0.01} _{-0.01} | 1.34 ^{+0.01} _{-0.01} | — | — |
| (a) J0453+1559 (Tauris & Janka 2019) | -17.1369 | 184.1245 | 0.522 | 1.559 ^{+0.005} _{-0.005} | 1.174 ^{+0.004} _{-0.004} | — | — |
| (a) J0509+3801 (Lynch et al. 2018) | -1.187 | 168.2747 | 1.9 | 1.34 ^{+0.08} _{-0.08} | 1.46 ^{+0.08} _{-0.08} | — | 0.15291 ± 0.00005 |
| (a) J0514-4002/NGC 1851 (Ridolfi et al. 2019) | -35.04 | 244.51 | 12.1 | 1.25 ^{+0.04} _{-0.05} | 1.22 ^{+0.06} _{-0.05} | — | — |
| (a) J0737-3039A (Yang et al. 2017; Kiziltan et al. 2013) | -4.5 | 245.24 | 1.1 | 1.381 ^{+0.007} _{-0.007} | 1.2489 ^{+0.007} _{-0.007} | — | — |
| (a) J0737-3039A (Kramer et al. 2021) | -4.5 | 245.27 | 1.1 | 1.388 ^{+0.002} _{-0.002} | 1.2489 ^{+0.007} _{-0.007} | — | — |
| (a) J0737-3039B (Yang et al. 2017; Kiziltan et al. 2013) | -4.5 | 245.24 | 1.1 | 1.2489 ^{+0.007} _{-0.007} | 1.337 ^{+0.05} _{-0.05} | — | — |
| (a) J0737-3039B (Kramer et al. 2021) | -4.5 | 245.24 | 1.1 | 1.248986 ^{+0.00013} _{-0.00013} | 1.337 ^{+0.05} _{-0.05} | — | — |
| (a) J1141-6545 (Bhat et al. 2008; Venkatraman Krishnan et al. 2020) | -3.86 | 295.79 | 10 | 1.27 ^{+0.01} _{-0.01} | 1.02 ^{+0.01} _{-0.01} | — | — |
| (a) J1518+0904 (Kiziltan et al. 2013) | 54.28 | 80.81 | 0.964 | 1.56 ^{+0.13} _{-0.11} | 1.05 ^{+0.15} _{-0.11} | — | 23.9 (Mignani et al. 2013) |
| (a) J1756-2251 (Ferdman et al. 2014) | 0.948010 | 6.498658 | 0.73 | 1.341 ^{+0.007} _{-0.007} | 1.230 ^{+0.007} _{-0.009} | — | 0.4435 |
| (a) J1757-1853 (Cameron et al. 2018) | 2.877 | 9.966 | 7.4 | 1.384 ^{+0.009} _{-0.009} | 1.3946 ^{+0.009} _{-0.009} | — | 0.130 |
| (a) J1757-1853 (Cameron et al. 2022) | 2.87698118 | 9.96611594 | 7.4 | 1.3406 ^{+0.005} _{-0.005} | 1.3922 ^{+0.005} _{-0.005} | — | — |
| (a) J1807-2500B/NGC 6544 (Alsing et al. 2018; Lynch et al. 2012) | -2.20605091 | 5.83588493 | 3 | 1.3655 ^{+0.002} _{-0.002} | 1.2068 ^{+0.002} _{-0.002} | — | — |
| (a) J1811-1736 (Zhang et al. 2011; Mignani et al. 2013) | 0.44 | 12.82 | 5.7 | 1.51 ^{+0.12} _{-0.11} | 1.06 ^{+0.45} _{-0.41} | — | 2.341 × 10 ⁻³ |
| (a) J1816+4510 (Kaplan et al. 2013) | 24.735 | 72.83 | 4.5 ^{+1.2} _{-1.2} Jennings et al. (2018) | 1.84 ^{+0.11} _{-0.11} | 0.193 ^{+0.02} _{-0.02} | — | — |
| (a) J1829+2456 (Haniewicz et al. 2020) | 15.6119 | 53.3426 | 0.915 | 1.306 ^{+0.007} _{-0.007} | 1.299 ^{+0.007} _{-0.007} | — | 13 |
| (a) J1903+0327 (Arzoumanian et al. 2018; Freire et al. 2008b) | -1.01 | 37.34 | 7 | 1.666 ^{+0.01} _{-0.01} | 1.033 ^{+0.01} _{-0.008} | — | 1.81 (Mignani et al. 2013) |
| (a) J1906-1746 (van Leeuwen et al. 2015) | 0.15 | 41.6 | 7.4 | 1.291 ^{+0.011} _{-0.011} | 1.322 ^{+0.011} _{-0.011} | — | 1.13 × 10 ⁻⁴ (Mignani et al. 2013) |
| (a) J1913+1102 (Ferdman et al. 2019) | 0.19 | 45.25 | 5.6 | 1.65 ^{+0.05} _{-0.05} | 1.24 ^{+0.05} _{-0.05} | — | — |
| (a) J1913+1102 (Ferdman et al. 2020) | 0.19357146 | 45.24993097 | 7.4 | 1.62 ^{+0.03} _{-0.03} | 1.0357 ^{+0.03} _{-0.03} | — | — |
| (a) J1930-1852 (Swiggum et al. 2015) | -16.87 | 19.98 | 2.004 | 1.27 ^{+0.11} _{-0.11} | 1.27 ^{+0.11} _{-0.11} | — | 0.163 |
| (a) J2222-0137 (Guo et al. 2021) | -46.0753 | 62.0185 | 0.268 | 1.81 ^{+0.03} _{-0.03} | 1.31 ^{+0.09} _{-0.09} | — | 30.6 |
| (a) LMC X-4 (Alsing et al. 2018) | -32.52909252 | 276.3349498 | 7.9 | 1.57 ^{+0.11} _{-0.11} | 1.29 ^{+0.05} _{-0.05} | — | — |
| (a) LMC X-4 (Bhalerao et al. 2022) | -32.52909252 | 276.3349498 | 7.9 | 1.285 ^{+0.05} _{-0.05} | 1.29 ^{+0.05} _{-0.05} | 7.76 ^{+0.32} _{-0.32} | — |
| (a) Sk 160/SMC X-1 (Alsing et al. 2018; Val Baker, A. K. F. et al. 2005) | -43.55935025 | 300.4149551 | 9 | 2.05 ^{+0.24} _{-0.23} | — | — | — |
| (a) Sk 160/SMC X-1 (Rawls et al. 2011) | -43.55935025 | 300.4149551 | 60.6 ^{+1.0} _{-1.0} | 1.037 ^{+0.08} _{-0.08} | 1.04 ^{+0.09} _{-0.09} | 15.70 ^{+1.36} _{-1.36} | — |
| (a) Sk 160/SMC X-1 (Bhalerao et al. 2022) | -43.55935025 | 300.4149551 | 60.6 | 1.32 ^{+0.16} _{-0.16} | — | — | — |
| (d1) J1537-5312 (Cameron et al. 2020) | 1.93548328 | 326.35139523 | 2.9 | 1.48 ^{+0.1} _{-0.1} | 0.1339705 ^{+0.00003} _{-0.00003} | — | 6.9 |
| (d1) J1547-5709 (Cameron et al. 2020) | -2.05222185 | 325.07635426 | 1.9 | 1.40 ^{+0.1} _{-0.1} | 0.20435198 ^{+0.00007} _{-0.00007} | — | 9.1 |
| (d1) J1618-4624 (Cameron et al. 2020) | 2.79197611 | 335.81590532 | 2.4 | 1.40 ^{+0.1} _{-0.1} | 0.7044464 ^{+0.00006} _{-0.00006} | — | 1.4 |
| (d1) J1727-2951 (Cameron et al. 2020) | 2.91863664 | 357.03727138 | 3.8 | 1.40 ^{+0.1} _{-0.1} | 0.01601 ^{+0.003} _{-0.003} | — | 30.2 |
| (d1) J1755-205 (Ng et al. 2015) | -0.34 | 3.76 | 10.3 | 1.35 ^{+0.1} _{-0.1} | 0.48 ^{+0.1} _{-0.1} | — | — |
| (d1) J1244-6359 (Ng et al. 2015) | 1.13414519 | 302.2037458 | 5.6 | 1.35 ^{+0.1} _{-0.1} | 0.68 ^{+0.1} _{-0.1} | — | 0.520 |
| (d1) J1101-6424 (Ng et al. 2015) | -4.0227463 | 291.41700154 | 4.5 | 1.35 ^{+0.1} _{-0.1} | 0.57 ^{+0.1} _{-0.1} | — | 44 |
| (d1) J1614-2230 (Ng et al. 2015) | 20.19 | 352.64 | 6.07 ^{+0.05} _{-0.05} Arzoumanian et al. (2018) | 1.35 ^{+0.1} _{-0.1} | 0.50 ^{+0.06} _{-0.06} | — | 5.2 |
| (b) 2A 1822-371/V* V691 CrA (Zhang et al. 2011; Bak Nielsen et al. 2017) | -11.29080163 | 369.1852 | 2.5 | 0.97 ^{+0.24} _{-0.24} | 0.33 ^{+0.05} _{-0.05} | — | — |
| (c) 4U 1822-371/V* V691 CrA (Alsing et al. 2018) | -11.29080163 | 368.5502712 | 2 | 1.96 ^{+0.36} _{-0.36} | — | — | — |
| (b) 4U 1538-52(cc) (Rawls et al. 2011) | 2.163693898 | 327.4196998 | 6.4 | 1.02 ^{+0.19} _{-0.17} | 16.4 ^{+5.2} _{-4.5} | — | — |
| (b) 4U 1538-52(cc) (Rawls et al. 2011) | 2.163693898 | 327.4196998 | 6.4 | 0.874 ^{+0.073} _{-0.073} | — | 15.72 ^{+0.32} _{-0.32} | — |
| (b) 4U 1538-52(cc) (Rawls et al. 2011) | 2.163693898 | 327.4196998 | 6.4 | 0.996 ^{+0.101} _{-0.101} | — | 12.53 ^{+2.11} _{-2.11} | — |
| (b) Cen X-3/V* V779 Cen (Alsing et al. 2011) | 0.335517538 | 292.0903507 | 5.7 | 1.21 ^{+0.12} _{-0.12} | 1.486 ^{+0.08} _{-0.08} | — | — |
| (b) Cen X-3/V* V779 Cen (Rawls et al. 2011) | 0.335517538 | 292.0903507 | 5.7 | 1.486 ^{+0.08} _{-0.08} | — | 12.56 ^{+0.36} _{-0.36} | — |
| (b) EXO 1722-363 (Fabanga et al. 2015) | -0.3539 | 351.4972 | 7.5 | 1.46 ^{+0.38} _{-0.38} | 13.6 ^{+1.6} _{-1.6} | 27.5 ^{+2.2} _{-2.2} | — |
| (b) EXO 1722-363 (Fabanga et al. 2015) | -0.3539 | 351.4972 | 7.5 | 1.91 ^{+0.45} _{-0.45} | — | 26.2 ^{+2.1} _{-2.1} | — |
| (b) J0405-7319 (Bell et al. 1995; Zhang et al. 2011) | -43.805 | 303.518 | 60.6 ^{+0.05} _{-0.05} Jennings et al. (2018) | 1.073 ^{+0.03} _{-0.03} | — | 31.82 ^{+0.28} _{-0.28} | — |
| (b) LMC X-4 (Zhang et al. 2011) | -32.52909252 | 276.3349498 | 7.9 | 1.31 ^{+0.14} _{-0.14} | 15.6 ^{+1.8} _{-1.8} | — | — |
| (b) Vela X-1/V* GP Vel (Zhang et al. 2011) | 3.929852619 | 263.0582983 | 1.8 | 1.88 ^{+0.13} _{-0.13} | 23.1 ^{+2.0} _{-2.2} | — | — |
| (b) Vela X-1/V* GP Vel (Fabanga et al. 2015) | 3.929852619 | 263.0582983 | 1.9 | 1.77 ^{+0.08} _{-0.08} | 0.35 ^{+0.1} _{-0.1} | — | — |
| (c) 4U 1656+35(Her X-1 (Alsing et al. 2018) | -0.8505 | 330.9263 | 5.8 | 1.77 ^{+0.03} _{-0.03} | — | 31.82 ^{+0.28} _{-0.28} | — |
| (c) B1257-12 (Konacki & Wolszczan 2003) | 75.414 | 311.31 | 0.709 | 1.40 ^{+0.14} _{-0.14} | — | 29.0 ^{+1.0} _{-1.0} | — |
| (c) B1620-26 (Thorsot et al. 1993) | 15.96 | 350.976 | 1.8 | 1.35 ^{+0.1} _{-0.1} | — | — | — |
| (c) B1829-10 | -0.597 | 21.587 | 4.685 | 1.40 ^{+0.1} _{-0.1} | — | — | — |
| (c) B1919+21 | 3.501 | 55.777 | 0.3 | 1.40 ^{+0.1} _{-0.1} | — | — | — |
| (c) Cyg X-7 | 2.1554 | 78.4883 | 6.1 | 1.40 ^{+0.19} _{-0.19} | 0.352 ^{+0.05} _{-0.05} | 13.25 ^{+1.37} _{-1.37} | — |
| (d1) Cyg X-2/V* V1341 Cyg (Alsing et al. 2018; Zhang et al. 2011) | -11.31636463 | 87.32819642 | 8 | 1.78 ^{+0.23} _{-0.23} | 0.60 ^{+0.13} _{-0.13} | — | — |
| (d1) Cyg X-2/V* V1341 Cyg (Casares et al. 2010) | -11.31636463 | 87.32819642 | 8 | 1.71 ^{+0.21} _{-0.21} | — | — | — |
| (c) EXO 0748-676 (Trigo et al. 2011) | -19.8109 | 279.9777 | 7.1 | 1.77 ^{+0.4} _{-0.4} | — | 16.6 ^{+1.8} _{-7.5} | — |
| (c) J1745-2912 (Schnitzeler et al. 2016) | -0.047 | 359.944 | 8.3 | 1.45 ^{+0.56} _{-0.56} | — | — | — |
| (c) J1745-2912 (Schnitzeler et al. 2016) | -0.175 | 359.788 | 8.109 | 1.45 ^{+0.56} _{-0.56} | — | — | — |
| (c) J1746-2849 (Schnitzeler et al. 2016) | -0.03 | 0.134 | 8.217 | 1.45 ^{+0.56} _{-0.56} | — | — | — |
| (c) J1746-2856 (Schnitzeler et al. 2016) | -0.233 | 0.126 | 8.149 | 1.45 ^{+0.56} _{-0.56} | — | — | — |
| (c) J1810-1744 (Roman et al. 2021) | -0.07 | 6.84 | 4 | 1.45 ^{+0.56} _{-0.56} | — | — | — |
| (c) J1810-1744 (Kandul & Roman 2023) | 16.806 | 44.642 | 3.03 | 2.13 ^{+0.04} _{-0.04} | 0.655 ^{+0.001} _{-0.001} | — | — |
| (c) J1812-1733 | 0.387 | 12.904 | 4.492 | 1.45 ^{+0.56} _{-0.56} | — | — | — |
| (c) J1825-1446 (Moldon et al. 2012) | -1.001 | 16.805 | 5.0 | 1.45 ^{+0.56} _{-0.56} | — | — | — |
| (c) KS 1731-260 (Özel et al. 2012) | 3.65256 | 10.7299 | 8 | 1.45 ^{+0.56} _{-0.56} | — | 13.5 ^{+2.0} _{-2.0} | — |
| (c) M13 A (Wang et al. 2020b) | 40.91351866 | 58.99966868 | 7.1 | 1.48 ^{+0.21} _{-0.21} | — | 11.04 ^{+1.0} _{-1.0} | — |
| (c) M13 C (Wang et al. 2020b) | 40.91268749 | 58.99528387 | 7.1 | 1.48 ^{+0.21} _{-0.21} | — | 11.04 ^{+1.0} _{-1.0} | — |
| (d1) M13 B (Wang et al. 2020b; Shaw et al. 2018) | 40.9127738 | 58.97105197 | 7.1 | 1.48 ^{+0.21} _{-0.21} | 0.1876 ^{+0.01} _{-0.01} | — | — |
| (d1) M13 D (Wang et al. 2020b; Shaw et al. 2018) | 40.90884273 | 59.00526155 | 7.1 | 1.48 ^{+0.21} _{-0.21} | 0.2085 ^{+0.01} _{-0.01} | — | — |
| (d1) M13 E (Wang et al. 2020b; Shaw et al. 2018) | 40.91029222 | 59.00755123 | 7.1 | 1.48 ^{+0.21} _{-0.21} | 0.0225 ^{+0.01} _{-0.01} | 11.04 ^{+1.0} _{-1.0} | — |
| (d1) M13 F (Wang et al. 2020b; Shaw et al. 2018) | 40.90293961 | 59.02801301 | 7.1 | 1.48 ^{+0.21</} | | | |

Table A2. Continuation of Table A1.

| Name | Gal. latitude, b , [deg] | Gal. longitude, l , [deg] | distance, [kpc] | NS mass, $[M_{\odot}]$ | Comp. star mass, $[M_{\odot}]$ | NS radius, [km] | Age τ_c [Gyr] |
|--|-------------------------------|--------------------------------|---|---|--|--------------------------------------|----------------------------|
| (d1) J1125+7819 (Lynch et al. 2018) | 37.895 | 128.289 | 0.903 | 1.35 ^{+0.1} _{-0.1} | 0.29 ^{+0.1} _{-0.1} | – | – |
| (d1) J1641+8049 (Lynch et al. 2018) | 31.763 | 113.840 | 3.035 | 1.35 ^{+0.1} _{-0.1} | 0.04 ^{+0.1} _{-0.1} | – | – |
| (d1) J1938+6604 (Lynch et al. 2018) | 20.030 | 97.946 | 3.380 | 1.35 ^{+0.1} _{-0.1} | 0.87 ^{+0.1} _{-0.1} | – | – |
| (d1) J0751+1807 (Furton et al. 2016; Freire et al. 2008b) | 21.09 | 202.73 | 1.07 ^{+0.24} _{-0.1} (Guillot et al. 2019) | 1.26 ^{+0.14} _{-0.11} | 0.12 ^{+0.02} _{-0.02} | 13.6 ^{+1.0} _{-1.0} | 8.0 |
| (d1) J0751+1807 (Desvignes et al. 2016) | 21.09 | 202.73 | 1.07 ^{+0.24} _{-0.1} (Guillot et al. 2019) | 1.64 ^{+0.15} _{-0.12} | – | – | – |
| (d1) J0955-6150 (Seryak et al. 2022) | -5.737093 | 283.684986 | 4.04 | 1.71 ^{+0.05} _{-0.02} | 0.254 ^{+0.002} _{-0.002} | – | 2.1 |
| (d1) J1012+5307 (Guillot et al. 2019; Mata Sánchez et al. 2020) | 50.86 | 160.35 | 0.907 ^{+0.131} _{-0.131} (Guillot et al. 2019) | 1.83 ^{+0.11} _{-0.11} | 0.16 ^{+0.02} _{-0.02} | – | – |
| (d1) J1012+5307 (Mata Sánchez et al. 2020) | 50.86 | 160.35 | 0.907 ^{+0.131} _{-0.131} (Guillot et al. 2019) | 1.78 ^{+0.16} _{-0.16} | – | – | – |
| (d1) J1022+1001 (Hobbs et al. 2004) | 51.1 | 231.79 | 0.645 | 1.7 ^{+0.3} _{-0.3} | 0.92 ^{+0.05} _{-0.05} | – | 6.01 (Mignani et al. 2013) |
| (d1) J1022+1004 (Reardon et al. 2016) | 51.10067364 | 231.79452981 | 0.645 | 1.7 ^{+0.3} _{-0.3} | 2.20 ^{+0.24} _{-0.24} | – | 6.0256 |
| (d1) J1022+1004 (Reardon et al. 2021) | 51.10067364 | 231.79452981 | 0.64 ^{+0.08} _{-0.08} | 1.4 ^{+0.5} _{-0.5} | 0.52 ^{+0.16} _{-0.16} | – | – |
| (d1) J1023+0038 (Shahbaz et al. 2019) | 45.78 | 243.49 | 1.368 ^{+0.042} _{-0.039} (Jennings et al. 2018) | 1.761 ^{+0.16} _{-0.16} | 0.241 ^{+0.02} _{-0.02} | – | – |
| (d1) J1023+0038 (Strader et al. 2019) | 45.78 | 243.49 | 1.37 ^{+0.04} _{-0.04} | 1.65 ^{+0.19} _{-0.19} | 0.22 ^{+0.03} _{-0.03} | – | – |
| (d1) J1045-4509 (Zhang et al. 2011) | 12.254 | 280.851 | 0.34 | 1.35 ^{+0.1} _{-0.1} | 0.19 ^{+0.1} _{-0.1} | – | – |
| (d1) J1045-4509 (Reardon et al. 2021) | 12.254 | 280.851 | 0.59 ^{+0.5} _{-0.58} | 1.35 ^{+0.1} _{-0.1} | 0.19 ^{+0.1} _{-0.1} | – | 6.76083 |
| (d1) J1227-4853 (Roy et al. 2015) | 13.8 | 298.97 | 1.4 | 0.86 ^{+0.13} _{-0.13} | 0.167 ^{+0.13} _{-0.13} | – | 2.4 |
| (d1) J1600-3053 (Arzoumanian et al. 2018) | 16.451 | 344.09 | 1.887 | 2.5 ^{+0.9} _{-0.9} | 0.34 ^{+0.09} _{-0.07} | – | – |
| (d1) J1600-3053 (Arzoumanian et al. 2018) | 16.451 | 344.09 | 1.887 | 2.3 ^{+0.7} _{-0.7} | 0.34 ^{+0.07} _{-0.07} | – | – |
| (d1) J1614-2230 (Verbic et al. 2008; Guillot et al. 2019) | 20.19 | 352.64 | 0.670 ^{+0.05} _{-0.04} (Arzoumanian et al. 2018) | 1.908 ^{+0.016} _{-0.016} | 0.493 ^{+0.003} _{-0.003} | 12.0 ^{+1.0} _{-1.0} | 1.2 |
| (d1) J1713-0747 (Arzoumanian et al. 2018) | 25.22 | 28.75 | 1.22 ^{+0.04} _{-0.04} (Arzoumanian et al. 2018) | 1.35 ^{+0.07} _{-0.07} | 0.292 ^{+0.011} _{-0.011} | – | – |
| (d1) J1713-0747 (Reardon et al. 2016) | 25.22884127 | 28.75055802 | 1.31 ^{+0.04} _{-0.04} | 1.70 ^{+0.13} _{-0.13} | 0.34 ^{+0.05} _{-0.05} | – | 8.51138 |
| (d1) J1713-0747 (Reardon et al. 2021) | 25.2288387 | 28.7505568 | 1.31 ^{+0.04} _{-0.04} | 1.28 ^{+0.08} _{-0.08} | 0.283 ^{+0.009} _{-0.009} | – | 8.51138 |
| (d1) J1738+0333 (Antoniadis et al. 2012) | 17.74 | 27.72 | 1.471 | 1.47 ^{+0.07} _{-0.07} | 0.181 ^{+0.007} _{-0.007} | – | 2.25 |
| (d1) J1740-5340 (NGC 6397 (20)) (Zhao et al. 2011; Keith et al. 2009; Orosz & van der Kerkwijk 2003) | -11.9669 | 338.1647 | 2.4 | 1.53 ^{+0.19} _{-0.19} | 0.181 ^{+0.1} _{-0.1} | – | – |
| (d1) J1741+1351 (Arzoumanian et al. 2018) | 21.641 | 37.885 | 1.667 | 1.14 ^{+0.43} _{-0.43} | 0.22 ^{+0.05} _{-0.04} | – | – |
| (d1) J1753-2240 (Zhang et al. 2011) | 1.663 | 6.299 | 3.232 | 1.25 ^{+0.2} _{-0.2} | 0.49 ^{+0.1} _{-0.1} | – | – |
| (d2) J1807-2459/NGC 6544 (Lynch et al. 2012) | -2.206 | 5.836 | 3 | 1.34 ^{+0.11} _{-0.11} | 0.0099 ^{+0.1} _{-0.1} | – | – |
| (d1) J1853+1303 (Corongiu et al. 2012) | 5.367 | 44.875 | 2.083 | 1.44 ^{+0.1} _{-0.1} | 0.33 ^{+0.37} _{-0.37} | – | – |
| (d1) J1909-3744 (Arzoumanian et al. 2018) | -19.6 | 359.73 | 1.00 ^{+0.04} _{-0.03} | 1.48 ^{+0.03} _{-0.03} | 0.208 ^{+0.002} _{-0.002} | – | – |
| (d1) J1909-3744 (Reardon et al. 2016) | -19.6 | 359.73 | 1.09 ^{+0.04} _{-0.03} | 1.47 ^{+0.03} _{-0.03} | 0.2067 ^{+0.0019} _{-0.0019} | – | 3.31131 |
| (d1) J1909-3744 (Reardon et al. 2021) | -19.6 | 359.73 | 1.15 ^{+0.04} _{-0.03} | 1.48 ^{+0.03} _{-0.03} | 0.2081 ^{+0.0009} _{-0.0009} | – | 3.31131 |
| (d1) J1910+1258 (Corongiu et al. 2012) | 1.795 | 46.564 | 1.496 | 1.6 ^{+0.6} _{-0.6} | 0.3 ^{+0.34} _{-0.34} | – | – |
| (d1) J1910+1258 (Nice et al. 2001) | -25.73 | 336.525 | 4 | 1.33 ^{+0.11} _{-0.11} | 0.18 ^{+0.08} _{-0.08} | – | – |
| (d1) J1918-0642 (Fonseca et al. 2016) | -9.12 | 30.03 | 1.16 ^{+0.02} _{-0.02} | 1.49 ^{+0.04} _{-0.04} | 0.219 ^{+0.012} _{-0.012} | – | 18 |
| (d1) J1918-0642 (Arzoumanian et al. 2018) | -9.12307649 | 30.02654694 | 4.71 | 1.15 ^{+0.07} _{-0.07} | 0.231 ^{+0.00} _{-0.00} | – | – |
| (d1) J1946+3417 (Jiang et al. 2021) | 1.79 | 69.29 | 6.94 | 1.83 ^{+0.02} _{-0.02} | 0.2659 ^{+0.003} _{-0.003} | – | – |
| (d1) J1946+3417 (Barr et al. 2017) | 4.71263925 | 69.29432913 | 5.1 | 1.828 ^{+0.02} _{-0.02} | 0.2656 ^{+0.002} _{-0.002} | – | 16 |
| (d1) J1949+3106 (Zhu et al. 2019; Fonseca et al. 2016) | 2.55336059 | 66.8583243 | 7.0 | 1.34 ^{+0.17} _{-0.17} | 0.81 ^{+0.06} _{-0.06} | – | 2.2 |
| (d1) J1950+2414 (Zhu et al. 2019) | -1.16874244 | 61.09752356 | 6.45 | 1.500 ^{+0.02} _{-0.02} | 0.28 ^{+0.05} _{-0.05} | – | 3.4 |
| (d1) J2016+1948 (Corongiu et al. 2012) | -8.675 | 60.522 | 2.162 | 1.05 ^{+0.5} _{-0.5} | 0.43 ^{+0.5} _{-0.5} | – | – |
| (d1) J2019+2425 (Nice et al. 2001) | -6.62 | 64.75 | 1.163 | 1.33 ^{+0.1} _{-0.1} | 0.33 ^{+0.1} _{-0.1} | – | – |
| (d1) J2019+2425 (Fonseca et al. 2016) | 38.217 | 41.051 | 1.515 | 4.42 ^{+0.1} _{-0.1} | 0.6 ^{+0.4} _{-0.4} | – | – |
| (d1) J2017+0609 (Fonseca et al. 2016) | -16.026 | 48.621 | 1.399 | 2.4 ^{+1.1} _{-1.1} | 0.32 ^{+0.16} _{-0.16} | – | – |
| (d1) J2043+1711 (Arzoumanian et al. 2018) | -15.3189035 | 61.91882154 | 1.6 ^{+0.2} _{-0.2} | 1.41 ^{+0.21} _{-0.21} | 0.175 ^{+0.06} _{-0.06} | – | – |
| (d1) J2302+4442 (Fonseca et al. 2016) | -14.005 | 103.395 | 0.863 | 5.3 ^{+2.2} _{-2.2} | 2.3 ^{+1.7} _{-1.7} | – | – |
| (d1) J2317+1439 (Fonseca et al. 2016) | -14.236018406 | 91.36074679 | 2.0 ^{+0.4} _{-0.3} (Arzoumanian et al. 2018) | 4.7 ^{+2.4} _{-2.4} | 0.7 ^{+0.5} _{-0.5} | – | – |
| (d1) J2045+3633 (McKee et al. 2020) | -3.92576397 | 77.832327 | 5.5 ^{+1.1} _{-1.1} | 1.25 ^{+0.021} _{-0.021} | 0.873 ^{+0.006} _{-0.006} | – | 0.84 |
| (d1) J2145+750 (Lohmer et al. 2004; Fonseca et al. 2016) | 1.30 | 86.86 | 4.12 | 1.20 ^{+0.014} _{-0.014} | 0.86 ^{+0.07} _{-0.07} | – | 1.15 |
| (d1) J2145+750 (Reardon et al. 2021) | 1.30 | 86.86 | 4.12 | 1.40 ^{+0.21} _{-0.21} | 0.86 ^{+0.07} _{-0.07} | – | 10.4 |
| (d1) J2234+0611 (Stovall et al. 2019) | -43.01 | 72.99 | 0.97 | 1.35 ^{+0.017} _{-0.017} | 0.298 ^{+0.013} _{-0.013} | – | – |
| (d1) XTE J2123-058/V ⁸ Lz Aqr (Alsing et al. 2011) | -36.1993 | 46.48299 | 8.5 | 1.46 ^{+0.39} _{-0.39} | 0.53 ^{+0.39} _{-0.39} | – | – |
| (d1) XTE J2123-058/V ⁸ Lz Aqr (Gelino et al. 2002) | -36.1993 | 46.48299 | 8.5 | 1.50 ^{+0.42} _{-0.42} | 0.49 ^{+0.17} _{-0.17} | – | – |
| (d2) B1516+02B/J1518+0204B (MSB) (Freire et al. 2008b; Zhang et al. 2011; Arzoumanian et al. 2018) | 46.806 | 3.859 | 7.5 | 2.08 ^{+0.19} _{-0.19} | 0.211 ^{+0.1} _{-0.1} | – | – |
| (d2) J0024-7204/B0021-72H (Tucmae) (Zhang et al. 2011) | -44.902 | 305.896 | 4.69 | 1.61 ^{+0.04} _{-0.04} | 0.18 ^{+0.06} _{-0.06} | – | – |
| (d2) J0024-7204/B0021-72H (Tucmae) (Zhang et al. 2011) | -44.903 | 305.9 | 4.9 | 1.41 ^{+0.1} _{-0.1} | 0.15 ^{+0.1} _{-0.1} | – | – |
| (d2) J1748-2021B/NGC 6440B (Zhang et al. 2011; Freire et al. 2008a) | 3.80168 | 7.72912 | 8.5 | 2.92 ^{+0.2} _{-0.2} | 0.12 ^{+0.1} _{-0.1} | – | – |
| (d2) J2045-750 (Lohmer et al. 2004; Fonseca et al. 2016) | 0.611 | 8.382 | 0.76 | 1.24 ^{+0.011} _{-0.011} | 0.78 ^{+0.04} _{-0.04} | – | – |
| (d2) J2045-750 (Reardon et al. 2021) | -5.58068 | 7.79821 | 5.6 | 1.61 ^{+0.007} _{-0.007} | 0.27 ^{+0.1} _{-0.1} | – | – |
| (d2) J2045-750 (Reardon et al. 2021) | -47.4425 | 143.961909 | 3.4 | 1.40 ^{+0.16} _{-0.16} | 0.18 ^{+0.02} _{-0.02} | – | – |
| (d2) J2045-750 (Reardon et al. 2021) | 1.69 | 3.84 | 6.9 | 1.32 ^{+0.1} _{-0.1} | 0.49 ^{+0.1} _{-0.1} | – | – |
| (d2) Ter Su/J1748-2446l (Kiziltan et al. 2013) | 1.69 | 3.84 | 6.9 | 1.87 ^{+0.32} _{-0.32} | 0.25 ^{+0.03} _{-0.03} | – | – |
| (d2) Ter Su/J1748-2446l (Kiziltan et al. 2013) | 1.69 | 3.84 | 6.9 | 1.728 ^{+0.18} _{-0.18} | 0.35 ^{+0.1} _{-0.1} | – | – |
| (d2) Ter Su/J1748-2446U (Kiziltan et al. 2013) | 1.69 | 3.84 | 6.9 | 1.73 ^{+0.11} _{-0.11} | 0.39 ^{+0.1} _{-0.1} | – | – |
| (d2) Ter SW/J1748-2446W (Kiziltan et al. 2013) | 1.69 | 3.84 | 6.9 | 1.69 ^{+0.1} _{-0.1} | 0.25 ^{+0.1} _{-0.1} | – | – |
| (d2) Ter SZ/J1748-2446Z (Kiziltan et al. 2013) | 1.69 | 3.84 | 6.9 | 1.48 ^{+0.1} _{-0.1} | 0.22 ^{+0.1} _{-0.1} | – | – |
| (c) IFGL J1417.7-4407 (Strader et al. 2019) | 16.14405096 | 318.8162599 | 3.1 | 1.62 ^{+0.43} _{-0.43} | 0.28 ^{+0.07} _{-0.07} | – | – |
| (c) PSR J1723-2837 (Strader et al. 2019) | 4.26007306 | 357.61630739 | 0.9 | 1.20 ^{+0.26} _{-0.26} | 0.36 ^{+0.08} _{-0.08} | – | – |
| (c) PSR J1219-0429 (Strader et al. 2019) | -36.9388023 | 48.91114168 | 1.83 | 1.74 ^{+0.018} _{-0.018} | 0.44 ^{+0.04} _{-0.04} | – | – |
| (c) PSR J2129-0429 (Bellm et al. 2016) | -36.9388023 | 48.91114168 | 1.83 | 1.74 ^{+0.008} _{-0.008} | 0.44 ^{+0.04} _{-0.04} | – | – |
| (c) PSR 2215+5135 (Strader et al. 2019) | -4.15873625 | 99.8673163 | 2.9 | 2.27 ^{+0.17} _{-0.17} | 0.33 ^{+0.03} _{-0.03} | – | – |
| (c) PSR J2329-0533 (Strader et al. 2019) | -52.99618205 | 92.29503519 | 1.1 | 1.63 ^{+0.25} _{-0.25} | 0.35 ^{+0.06} _{-0.06} | – | – |
| (c) PSR J2339-0533 (Strader et al. 2019) | -52.99618205 | 92.29503519 | 1.87 ^{+0.01} _{-0.01} | 1.47 ^{+0.09} _{-0.09} | 0.27 ^{+0.02} _{-0.02} | – | – |
| (c) 3FGL J0212.1+5320 (Strader et al. 2019) | -7.2098713 | 134.92218842 | 1.16 | 1.85 ^{+0.26} _{-0.26} | 0.50 ^{+0.19} _{-0.19} | – | – |
| (c) 2FGL J0846.0+2820 (Swihart et al. 2017) | 28.14467583 | 131.5911488 | 8.1 | 1.90 ^{+0.041} _{-0.041} | 0.77 ^{+0.02} _{-0.02} | – | – |
| (c) 3FGL J2039.6-5618 (Strader et al. 2019) | -37.1453325 | 341.26527565 | 3.4 | 2.04 ^{+0.37} _{-0.37} | 0.47 ^{+0.21} _{-0.21} | – | – |
| (c) 3FGL J0427.9-6704 (Strader et al. 2019) | -38.55416428 | 279.13812847 | 2.4 | 1.86 ^{+0.011} _{-0.011} | 0.65 ^{+0.08} _{-0.08} | – | – |
| (c) 3FGL J0427.9-6704 (| | | | | | | |

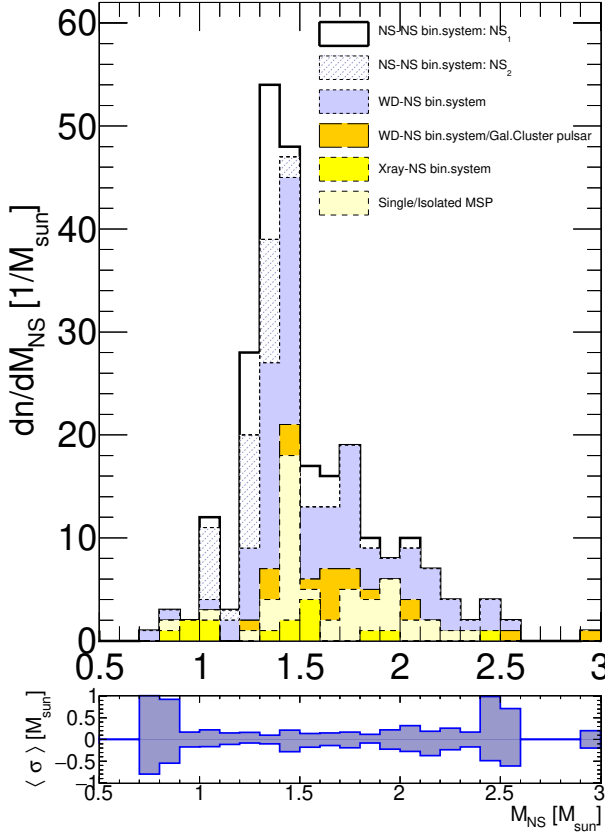


Figure B1. Mass distribution of the examined NSs. Full set includes binary systems such as NS-NS, WD-NS, Xray-NS, and single Millisecond Pulsars (MSPs). Bottom pad shows the average uncertainty in the NS mass measurements.

APPENDIX B: NEUTRON STARS MASS REPORT RACE.

We have revised our plots to address the missing NSs and incorporate updated mass reports for previously examined NSs. Additional entities have been taken from Ref. Shao et al. (2020), see gray lines in Tables A1–A2. Importantly, it is noteworthy that the inclusion of additional NSs has not made a significant influence on the overall findings and outcomes presented in our paper.

This paper has been typeset from a $\text{\TeX}/\text{\LaTeX}$ file prepared by the author.

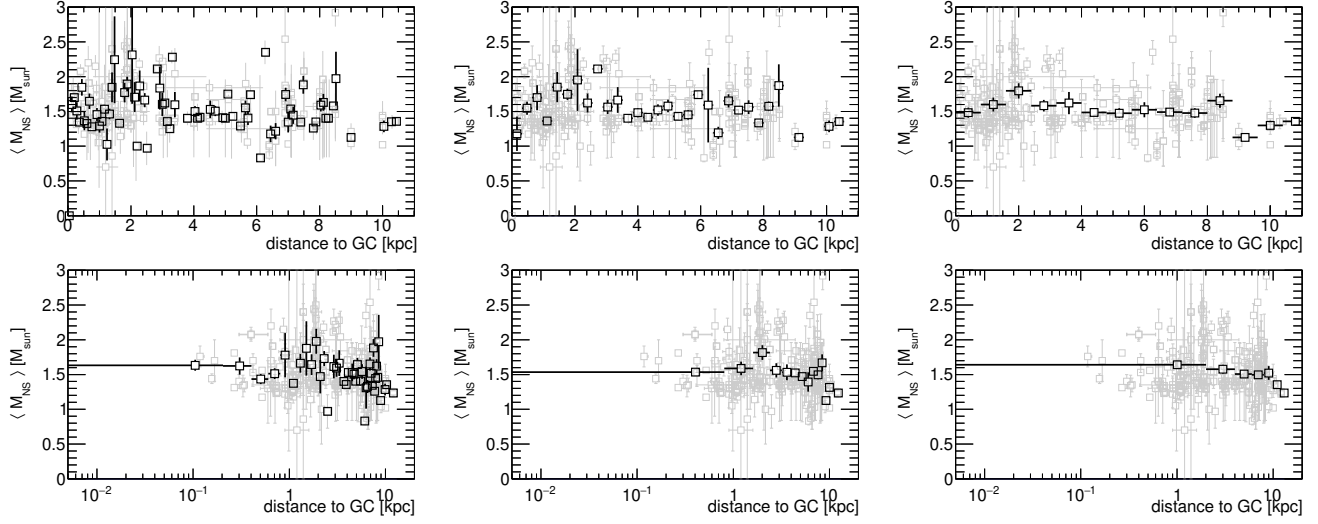


Figure B2. Mass distribution of the examined NSs as a function of the distance to Galactic centre. Black boxes - the average mass and radius, the vertical error bars simply reflect the statistical uncertainty at the given bin; light grey boxes - the measured masses and radii of the NSs with the measured uncertainties, see Tables A1-A2. We show three different profiles using 2000, 500, and 200 bins from 0 to 20 kpc (from top to bottom) to plot the average mass distribution. Top: distance shown in linear scale. Bottom: in log scale.

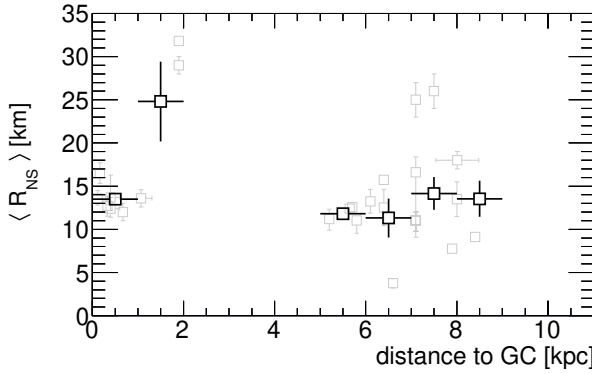


Figure B3. Radius distribution of the examined NSs as a function of the distance to Galactic centre. Black boxes - the average mass and radius, the vertical error bars simply reflect the statistical uncertainty at the given bin; light grey boxes - the measured masses and radii of the NSs with the measured uncertainties, see Tables A1-A2.

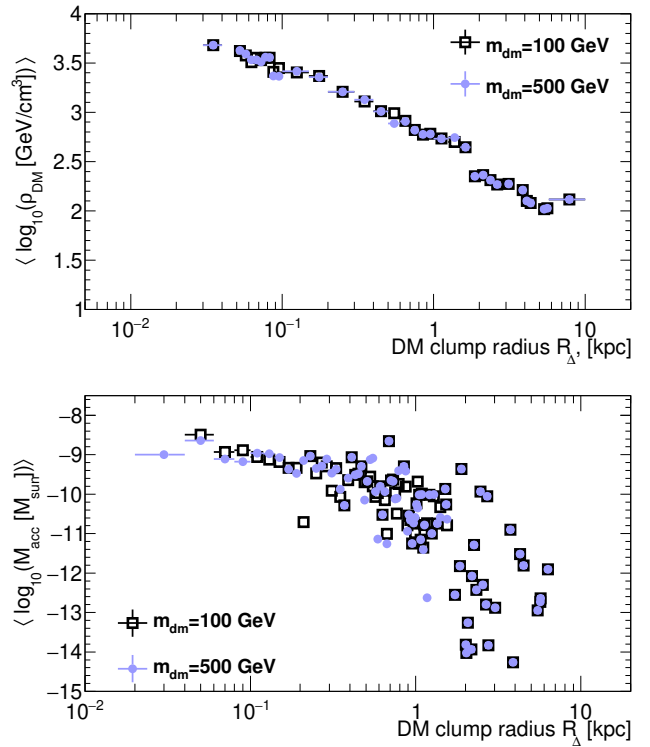


Figure B4. Top: DM density distribution in a minihalo/clump. Bottom: Accreted DM mass in a minihalo/clump, computed with the help of Eq.(11), where DM density distribution in a minihalo/clump, was computed from the Einasto profile using the ρ_s and r_s values for the selected clump associated to the NS taken from CLUMPY simulation. The results are shown for galaxy models assuming $m_{\text{dm}} = 100$ and 500 GeV. We used only those clumps that are associated with the NS.

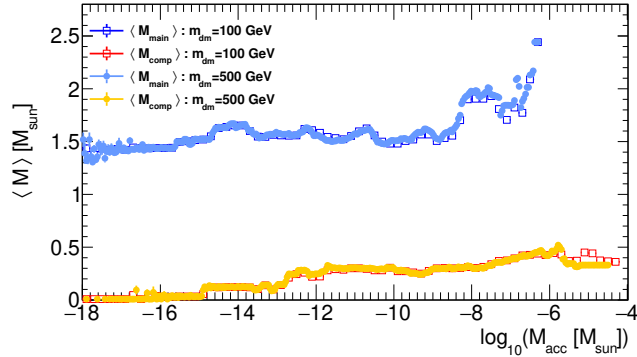


Figure B5. Change of the average star (NS/WD) mass with respect to the DM mass accreted inside the selected clumps, where the accreted mass was computed with the help of Eq.(11). Results for the clumps obtained assuming particle mass $m_{\text{md}} = 100 \text{ GeV}$ (box) and 500 GeV (circles). The profiles are shown for the main star (azure,blue) and companion star separately (red, orange).

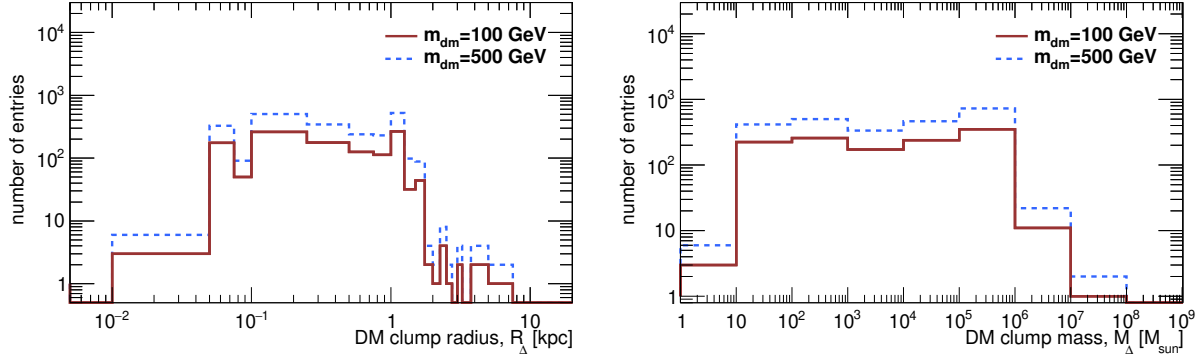


Figure B6. (left): The outer bound of the DM-clumps in the vicinity of the examined. (right): The mass of the DM clumps in the vicinity of the examined NSs in absolute units. The real-space distance between NSs and DM clumps coordinates should be less than 0.01, 0.05, 0.1, 0.25, 0.5, 0.75, 1, 2, and 5 kpc, while the scale of the selected clumps should be greater than the distance.

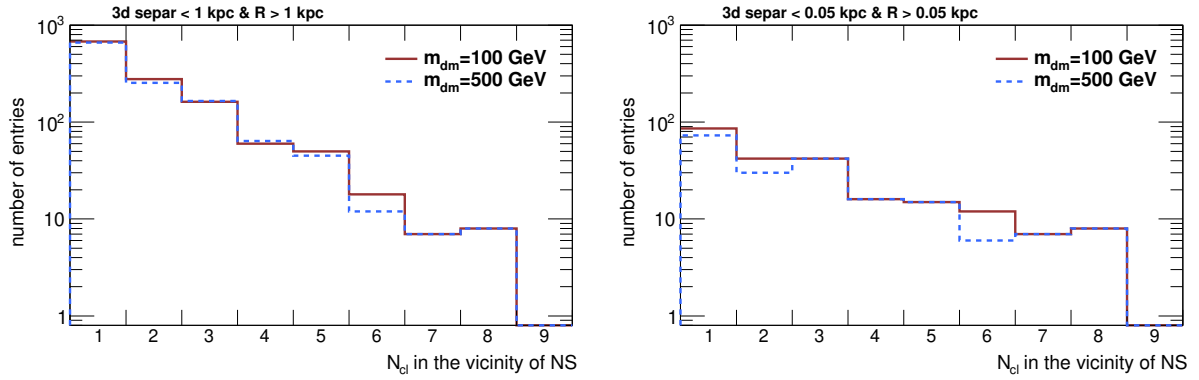


Figure B7. The number of DM clumps in the vicinity of the examined NSs in absolute units. (left): The multiplicity of DM clumps in the vicinity of the NSs when the real space separation distance between DM clumps and NSs coordinates should be less than 1 kpc, while the scale of the selected clumps should be greater than 1 kpc. (right): The distance between NSs and DM clumps coordinates should be less than 0.05 kpc, while the scale should be greater than 0.05 kpc.

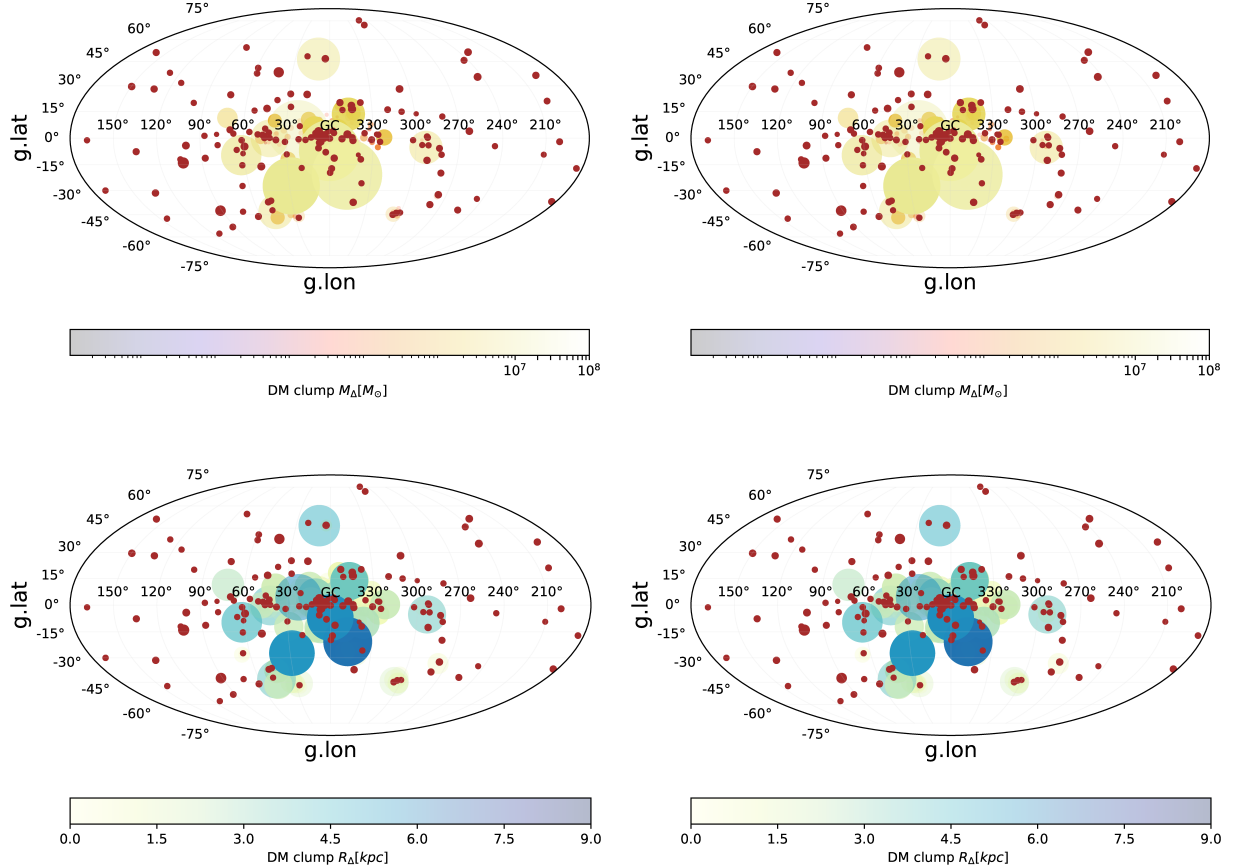


Figure B8. The distribution of DM clumps mass (top) and outer bound radius (bottom), as seen projected on the sky in Galactic coordinates. DM clumps were selected with respect to the 3d-distance and scale. Namely, the 3d-separation distance should be less than 0.05 kpc, and the radius of the selected clump should be greater than 0.05 kpc. The circle size indicates the mass of the DM clump (top), and the scale of the DM clumps (bottom). Red data points indicate known NSs. (left) CLUMPY simulation using $m_{\text{md}} = 100 \text{ GeV}$; (right) $m_{\text{md}} = 500 \text{ GeV}$.

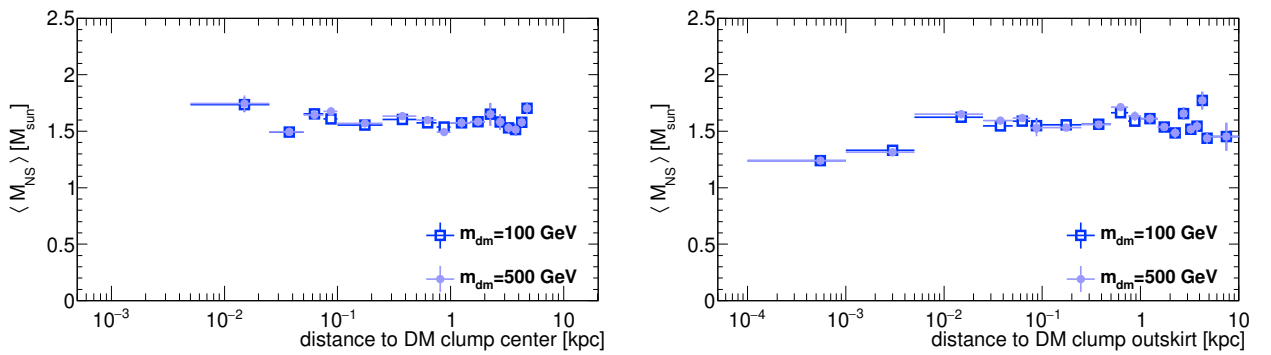


Figure B9. Left: The distribution of NS mass inside the DM clumps as function of distance to the clump center. Right: The distribution of NS mass inside the DM clumps as function of distance to the clump outskirt. Results are shown for the DM clumps produced with the help of CLUMPY assuming $m_{\text{md}} = 100 \text{ GeV}$ (boxes); $m_{\text{md}} = 500 \text{ GeV}$ (circles).

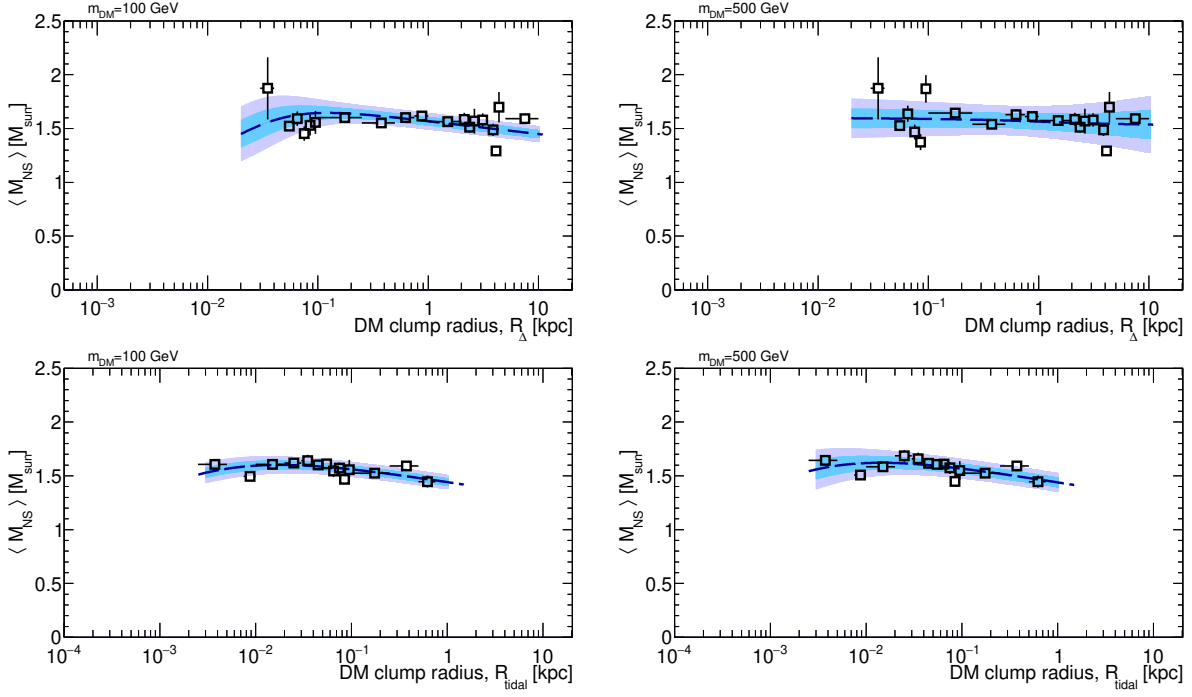


Figure B10. Fits to the NSs mass as a function of the clump radius (top) and tidal clump radius (bottom). Clumps were selected in the vicinity of 0.01, 0.05, 0.1, 0.25, 0.5, 0.75, 1, 2, and 5 kpc to the NSs, clumps scale was requested to be greater than this separation distance. Left: using the DM mass $m_{\text{dm}} = 100 \text{ GeV}$. Right: using the DM mass $m_{\text{dm}} = 500 \text{ GeV}$.

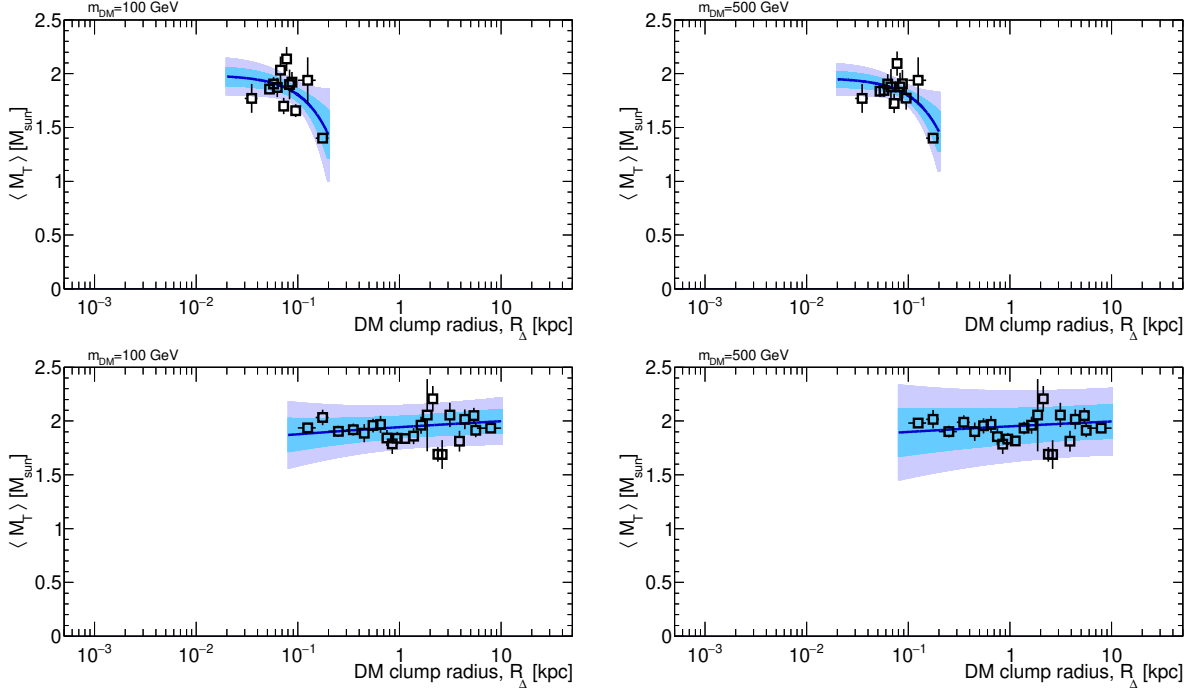


Figure B11. Fits to the total mass of the binary systems as a function of the clump radius. Top: Clumps were selected in the vicinity of 0.05 kpc to the NSs, clumps scale was requested to be greater than this separation distance ($> 0.05 \text{ kpc}$). Bottom: Clumps were selected in the vicinity of 0.1 kpc to the NSs, clumps scale was requested to be greater than this separation distance ($> 0.1 \text{ kpc}$). Left: using the DM mass $m_{\text{dm}} = 100 \text{ GeV}$. Right: using the DM mass $m_{\text{dm}} = 500 \text{ GeV}$. Fits performed with the help of the power law function.